

Wound Healing Effects of a Modified Collagen-Binding Antimicrobial Peptide LL37

A Major Qualifying Project Report submitted to the Faculty of
Worcester Polytechnic Institute
in partial fulfillment of the requirements for the
Degree of Bachelor of Science

By:

Megan Dion

December 2015

Project Number: TAC-AASP

Professor Terri Camesano, Advisor

Acknowledgements

First I would like to thank my advisor, Professor Terri A. Camesano for providing me with support and guidance through the project work as well as providing me the opportunity to work on this project.

Next, I would like to thank Ph. D. candidate Lindsay Lozeau for her advice, assistance, and training. Her help and numerous suggestions truly made this project successful and I hope this projects results will help her in the future.

I would like to thank Dr. Tanja Dominko who provided me with CT 1005 Fibroblast Cells and Dr. Denis Kole who provided me with recombinantly derived *c*CBD -LL37, *f*CBD-LL37, and wild-type conditioned media. I would like to thank Professor Sakthikumar Ambady from the Worcester Polytechnic Institute Biomedical Engineering Department for allowing me to use his fluorescence microscope to take pictures for my wound healing assays. Also, I would like to thank Professor Marsha Rolle for her input and ideas on the project.

Finally, I would like to thank WPI undergraduate student Nick Bergstrom for developing the ImageJ program for analyzing the percent area and the rest of the Camesano lab group for all their help.

Abstract

Chronic wounds can often become infected due to bacterial resistance towards antibiotics and a new potential solution to this resistance is to use antimicrobial peptides (AMPs) to heal wounds. The goal of this project was to determine the wound healing ability of using antimicrobial peptides (AMPs) and modified collagen-binding AMPs on the ability of cells to migrate over in a bare area on a dish, simulating migration at the wound site, at varying AMP concentrations over time using scratch assays. In these assays, 3 peptides were studied for their ability to stimulate migration in human fibroblasts (CT 1005): human-derived AMP LL37, a modified synthetic LL37 with a collagen-binding domain (cCBD-LL37), and recombinant cCBD-LL37 produced and harvested from H1299 human lung carcinoma cells. The results showed that any concentration of AMP had a wound closure rate than the no AMP control, the cCBD-LL37 healed at a slower rate than LL37 and the no AMP control, and conditioned media healed at a faster rate than a control with no conditioned media. The concentrations of AMPs studied will be valuable in the development of an AMP-tethered collagen-based scaffolding material to help with the healing of chronic wounds.

Table of Contents

Acknowledgements	2
Abstract	3
Table of Contents	4
Table of Figures.....	6
Introduction.....	1
Background.....	4
Chronic Skin Wounds.....	4
Microbial Diversity of the Chronic Wound Environment	5
Current Forms of Treatment.....	7
Development of a New Antimicrobial Therapy.....	10
Antimicrobial Peptides (AMPs) and Human Cathelicidin LL37	11
Modified Collagen-Binding LL37 Design.....	13
Scratch Assay	15
Materials and Methods.....	16
Materials.....	16
Cell Culture Methods.....	16
<i>Baseline, (-)AMP Control</i>	17
<i>Sample, (+)AMP, Synthetic LL37 and cCBD-LL37 AMP</i>	18
<i>Sample, (+)AMP, Recombinant cCBD-LL37 & fCBD-LL37</i>	18
Imaging.....	19
Data Analysis.....	19
<i>Scratch Width Scratch Assay Results</i>	20
<i>Percent Area of Wound</i>	20
<i>Wound Closure Rate: By Scratch Width and By Area</i>	21
Error.....	21
Statistical Significance	22
Rationalizing Concentration Choice.....	23
Results.....	24
<i>Controls</i>	24
<i>(+) Synthetic LL37 and cCBD-LL37 AMP Scratch Assay Results</i>	25
<i>Recombinant cCBD-LL37 & fCBD-LL37 and WT CM Scratch Assay Results</i>	31
<i>Wound Closure Rate</i>	33
Discussion.....	38
<i>Controls</i>	38
<i>(+) Synthetic LL37 and cCBD-LL37 AMP Results</i>	38
<i>Wound Closure Rate</i>	42
<i>Sources of Error</i>	42
<i>Overall Recommendations for ECM Incorporation of AMPs</i>	42

Conclusions.....	44
References	46
Appendices.....	48
Appendix A: Background Figures.....	48
Appendix B: Scratch Width, Percent Area, and Wound Closure Rate Summarized Data...	50
<i>Scratch Width Results</i>	50
<i>Percent Area Results</i>	52
<i>Wound Closure Rate Results</i>	54
Appendix C: ImageJ Program*	54
Appendix D: Troubleshooting Guide	56

Table of Figures

Figure 1.....	4
Figure 2.....	5
Figure 3.....	6
Figure 4.....	8
Figure 5.....	48
Figure 6.....	49
Figure 7.....	49
Figure 8.....	12
Figure 9.....	14
Figure 10.....	15
Figure 11.....	20
Figure 12.....	22
Figure 13.....	23
Figure 14.....	24
Figure 15.....	25
Figure 16.....	26
Figure 17.....	27
Figure 18.....	28
Figure 19.....	28
Figure 20.....	29
Figure 21.....	29
Figure 22.....	30
Figure 23.....	30
Figure 24.....	31
Figure 25.....	32
Figure 26.....	32
Figure 27a.....	33
Figure 27b.....	34
Figure 27c.....	34
Figure 27d.....	35
Figure 28a.....	35
Figure 28b.....	36
Figure 28c.....	36
Figure 28d.....	37

Introduction

In the United States alone, \$25 billion is spent annually on the treatment of chronic wounds, negatively impacting 6.5 million patients (Sen et al., 2009). Individuals with diabetes and obesity often develop chronic wounds due to their weakened immune systems and the prevalence of these diseases is rising. When a skin wound fails to heal within a period of approximately three months it is considered a chronic wound. The inability of wounds to heal can also cause a lot of pain and lower quality of life for the patients affected. Patients who develop chronic wounds suffer from persistent inflammation and are often infected with microbes such as bacteria and fungi (Duplantier & van Hoek, 2013). If a wound becomes infected, the body's immune system becomes hindered and can take a much longer time period to heal the wound. Further, the rise of antibiotic resistance, considered to be a "catastrophic threat to human health" by the Centers for Disease Control and Prevention (CDC), is severely complicating treatment of chronic wounds (CDC, 2014). Over 2 million antibiotic resistant infections occur in the United States each year, resulting in 25,000 deaths (*Discharges of Inpatients from Nonfederal Hospitals*, 2010). Current treatments for chronic wounds lack the adequate broad-spectrum antimicrobial activity needed for such diverse microbial environments while combating antibiotic resistance and promoting wound healing.

For chronic wounds, extracellular matrix (ECM)-based artificial and natural scaffolding materials, the most common of which are collagen-based, are used to cover the area and keep it moist in order to aid healing. Once infected, the gold standard of treatment is antibiotic use, but as antibiotic use increases so does the resistance of bacteria. Widespread overuse of antibiotics in hospitals and other care facilities have made these particularly dangerous places for developing infections. Specialized sterilization procedures have been developed by the CDC in

order to help prevent the number of wound infections, but new therapies to combat the resistance already occurring are needed ("Guideline for Disinfection and Sterilization in Healthcare Facilities," 2009).

Antimicrobial peptides (AMPs) have recently been considered as viable alternative broad-spectrum antimicrobials that may help to heal wounds (Durr, Sudheendra, & Ramamoorthy, 2006). AMPs are part of many organisms' innate immunities, have broad-spectrum antimicrobial activity even against resistant organisms. Some AMPs, such as the human-derived LL37, have been shown to promote wound healing (Durr et al., 2006). Unfortunately, few AMP therapies are on the market due to problems with toxicity to cells, stability, and high manufacturing costs (Kim, Jang, Kim, & Cho, 2013). To overcome these limitations, our approach is to tether AMPs to collagen in order to target their activity in a local wound healing scaffold to prevent infection and promote healing.

Main considerations for novel, AMP-based chronic wound healing treatments are biocompatibility and ability to promote healing. The **long-term goal of this project is** to use recombinant cells to create collagen-based ECM scaffolding biomaterials functionalized with *c*CBD-LL37 and/or *f*CBD-LL37 that will help promote healing and prevent wound infection in chronic wounds. Preliminary activity, toxicity and collagen-binding studies of this AMP have been done with synthetic *c*CBD-LL37, synthetic LL37, and both recombinant AMPs, *c*CBD-LL37 and *f*CBD-LL37. **In this project**, these AMPs were tested in solution for the ability to promote healing of CT 1005 fibroblasts *in vitro* over time at concentrations of 0.05- μ M, 3- μ M, and 12- μ M using scratch assays. **Our hypothesis** is that the addition of the *c*CBD moiety in the synthetic AMPs and both *c*CBD and *f*CBD moieties in recombinant AMPs will not be significantly different than unmodified LL37 at any of the concentrations, and that the highest

migration of the fibroblasts will be observed at the middle concentration (3- μ M). The results of this project could be used to help develop a new antimicrobial treatment for healing and preventing infection in chronic wounds.

Background

Chronic Skin Wounds

Chronic wounds are those that have failed to proceed through the reparative process of wound healing in order to return anatomic and functional integrity to the injured site within a time period of 3 months (Regan & Barbul). There are 4 phases to the wound healing process; the hemostasis phase, inflammatory phase, proliferative phase, and maturation phase. Each phase has a specific function in the wound healing process as described in **Figure 1**.

4 Phases of wound healing

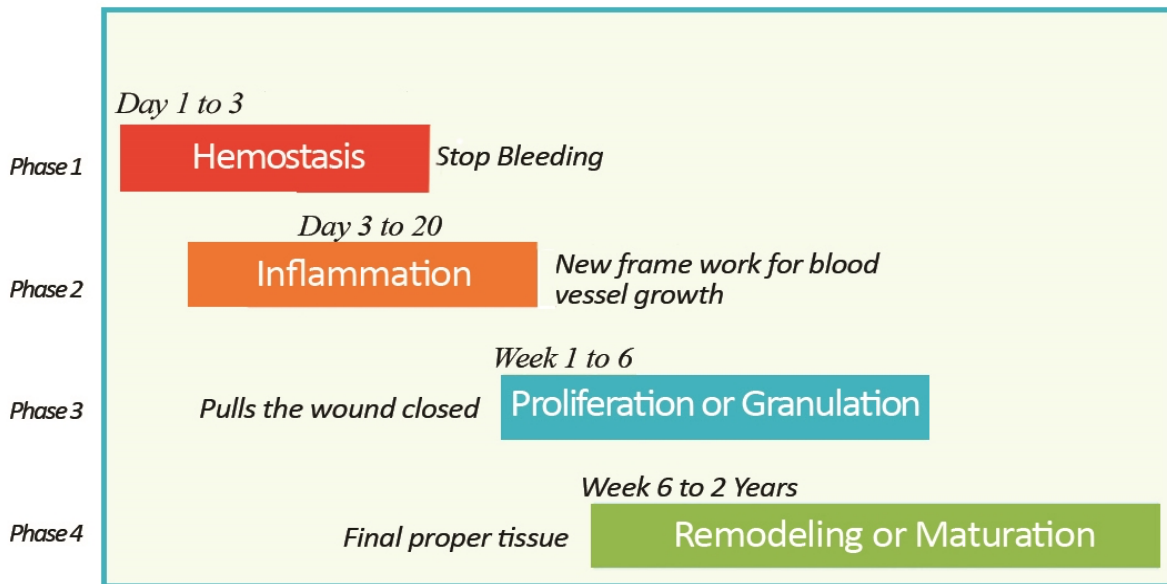


Figure 1: The four phases in the wound healing process are the hemostasis, inflammatory, proliferative, and maturation phases. A normal wound proceeds through each step to heal while a chronic wound remains in the inflammatory phase, for an extended period of time ("Essentials of Wound Healing," 2015).

A chronic wound is continuously in the inflammatory phase; thus, the pain for the patient and lowered quality of life during treatment lasts considerably longer. Conditions including poor blood supply or low oxygen, infection, weakened immune systems, and tissue swelling may also lead to the development of a chronic wound ("Chronic Wound Care," 2015). Individuals with

other health conditions such as diabetes and obesity suffer a higher risk of developing chronic wounds in this way, also causing complicated treatments ("Chronic Wound Care," 2015).

Microbial Diversity of the Chronic Wound Environment

The microbial diversity of chronic wounds (**Figure 2**) makes development of suitable multi-functional and broad-spectrum antimicrobial therapy challenging (Lipsky & Christopher, 2009).

Bacterial genus	Type of wound (specimen)					
	Mixed ^a		Venous ulcers (tissue specimens) ^b		Chronic wounds ^c	
	Chronic (tissue)	Acute (biopsy)	Healers	Nonhealers	Swab culture	Tissue PCR
<i>Staphylococcus</i>	65	60	100	100	28	68
<i>Enterococcus</i>	62	80	12	18
<i>Pseudomonas</i>	35	20	88	70	32	28
<i>Proteus</i>	24	20	25	30	126	...
<i>Citrobacter</i>	24	20	8	28
<i>Enterobacter</i>	24	20
<i>Streptococcus</i>	22	0	25	60
<i>Micrococcus</i>	25	90
<i>Escherichia</i>	14	0
<i>Morganella</i>	8	0
<i>Klebsiella</i>	5	0
<i>Acinetobacter</i>	5	0
<i>Serratia</i>	3	0
<i>Corynebacteria</i>	0	68
Anaerobes	50	40	0	70

NOTE. Data are from [12, 13].

^a Diabetic foot, pressure, or venous stasis ulcers (77 chronic and 16 acute); several anaerobic organisms detected by molecular methods but none were isolated by culture [12].

^b Specimens from 8 healing and 10 nonhealing chronic venous leg ulcers; 40% of species detected by molecular methods were not detected by standard culture [13].

^c Specimens from 19 wounds (all but 1 of the lower extremity) [14].

Figure 2: The vast diversity of different bacterial species found in venous ulcers and chronic wounds. Eight healing and 10 non-healing venous ulcers were tested and 19 chronic wounds were tested for different types of microbial species (Lipsky & Christopher, 2009).

The existence of complex bacterial communities residing on surfaces, called biofilms, have increased antibiotic resistance, induction of inflammation and pathogenesis due to secreted extrapolymeric substances (

Figure 3) and can delay healing even further (Duplantier 2013). Biofilm-forming microbes persist in adhesive polymeric matrices that can severely complicate treatments.

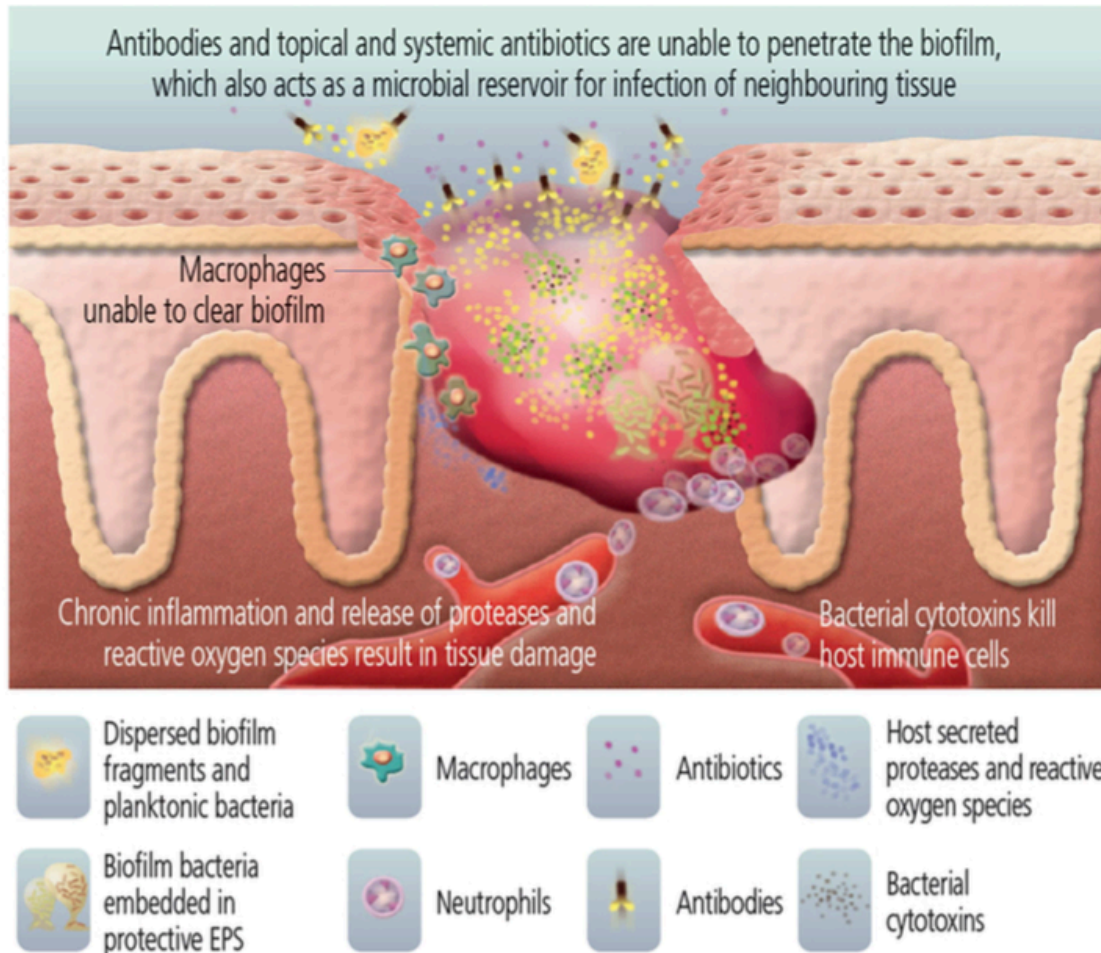


FIGURE 3 | Bacteria in the wound are protected by biofilm. [Image used with permission from Biofilms Made Easy, 2010, Vol. 1, Issue 1, published on Wounds International (http://www.woundsinternational.com/pdf/content_8851.pdf)].

Figure 3: Bacterial biofilm formation in a skin wound environment. A cascade of responses by the host’s immune system is triggered in an attempt to heal the wound. Antibiotics are also unable to heal the wound because they are unable to penetrate the biofilm and the secreted extra polymeric substances (EPS) (Duplantier & van Hoek, 2013).

Hospitals are a particularly dangerous breeding ground for the development of antibiotic resistant bacteria. Infections also often contain multiple microbial species of bacteria that live cooperatively in highly organized biofilms which means that antibiotic therapy that targets

specific bacteria is ineffective in treating these wounds and an individual's immune response is also ineffective (Duplantier & van Hoek, 2013).

The occurrence of resistant microbes in chronic wound infections is commonly developed in hospitals and care facilities due to their increased use of antibiotics. Detailed sterilization procedures from the CDC are provided in order to help prevent wound infection. These procedures depend on whether the procedure is critical, semi-critical, or post-operative care. The most common procedures require care facilities to meticulously clean patient-care items with water and detergent, or with water and enzymatic cleaners before high-level disinfection or sterilization procedures with ultrasonic cleaners, washer-disinfectors, or washer-sterilizers are used ("Guideline for Disinfection and Sterilization in Healthcare Facilities," 2009). Although these procedures reduce the number of antibiotic resistant bacteria, there is a strong need to develop new antibiotics to replace current treatments.

Current Forms of Treatment

One of the most important factors when deciding how to treat a skin wound is the depth of the wound. There are two general ways to classify wounds; partial-thickness or full-thickness. An injury that extends through a portion of the dermis is considered a partial-thickness wound while wounds that extend through the entire dermis and parts of the subcutaneous layer are considered full-thickness wounds as shown in Figure 4.

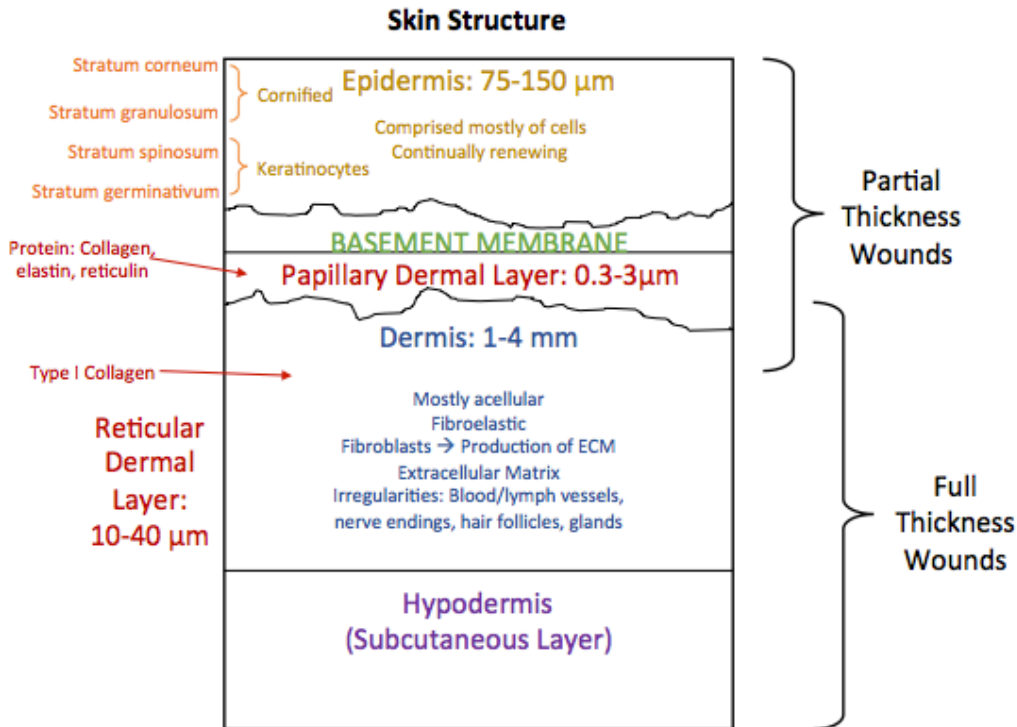


Figure 4: Depiction of the layers of the skin and the distinction between where a partial thickness or full thickness skin wound would be classified.

Many partial-thickness wounds can be treated with topical medications and dressings but most full-thickness wounds require localized regenerative therapies in order to heal the wound, including debridement and skin grafting (Hyakusoku, Orgill, Teot, Pribaz, & Ogawa, 2010). It is important to treat the wound quickly because when it is left untreated, damaged tissue begins to break down and becomes susceptible to bacterial infection (James, Booth, Gilbert, Jones, & Shevchenko, 2008). **The main drawback of available wound dressings for chronic wound treatment is the absence of broad-spectrum antimicrobial activity to combat over 200 species of bacteria that can reside in a single chronic wound** (Dowd et al., 2008).

Topical Antimicrobial Therapies

Today, clinicians consider using topical antimicrobials for individuals who have partial-thickness chronic wounds (Lipsky & Christopher, 2009). Topical antimicrobials have been

traditionally made as ointments and creams with antibiotics or antiseptics. Several advantages and disadvantages to using topical antimicrobials are outlined in Figure 5 in Appendix A (Lipsky & Christopher, 2009). Overall, ointments are more occlusive, often contain petrolatum, and are best for dry lesions while creams are less occlusive, wash off with water, are cleaner, and are best for moist lesions. Newer technologies have incorporated antimicrobials into dressings to allow controlled release at the wound surface over time. The major problem with these topical therapies is that there are no specific tests outlined by any agency in order to standardize and evaluate their efficacy (Lipsky & Christopher, 2009). Also, those treatments that are released have sub-optimal concentrations that promote resistance in bacteria. Figure 6 in Appendix A shows current topical antimicrobial wound treatments along with their advantages and disadvantages (Lipsky & Christopher, 2009). These treatments are not used for full-thickness wounds.

Debridement

One of the main forms of treatment for full-thickness chronic wound infections is debriding the wound to remove anything from the wound that can delay healing and lead to infection. This includes dead tissue, infected tissue, and other debris ("Chronic Wound Care," 2015). Common methods of debridement include surgical removal of the affected tissue, hydration or absorption to change moisture of the wound, and chemical breakdown of any dead tissue around the wound (Shai & Maibach, 2005). This treatment is incredibly painful and expensive for the patient and hospitals to undertake.

Skin grafting

Skin grafting is another form of treatment that is used when significant skin loss has occurred in order to support functional regeneration of the dermis especially near joints (Shai &

Maibach, 2005). Skin grafts are used for wound coverage or wound closure for full-thickness wounds. Most skin grafts are called *autografts* where healthy skin is taken from the patient's own body and transplanted to the wound site in order to remove the obstacle of finding a donor and limit immunological rejection; however, this is not always an option for the immunocompromised patient. An example is in burn victims where a large portion of their skin is charred, leaving limited healthy skin to harvest (James et al., 2008). Commercial scaffolding materials are usually made of synthetic polymers such as polyactic acid (PLA), polyglycolide (PGA), and copolymers or naturally-derived structural proteins, such extracellular matrix (ECM) (Dhandayuthapani, Yoshida, Maekawa, & Kumar, 2011). The ECM is an attractive target for localizing exogenous peptide signaling molecules because it stores various skin growth factors that the AMP could use to help heal a wound. A high percentage of ECM-based dressings are collagen-based, the most abundant structural protein in the body (Brett, 2008). Many leading companies use collagen-based wound dressings such as Integra, Organogenesis, and Johnson and Johnson, Smith and Nephew, and LifeCell.

Development of a New Antimicrobial Therapy

There is a strong need to develop new antibiotics and clinicians and industry both have defined the ideal antimicrobial agent, outlined in Figure 7 in Appendix A. This agent would target the specific antimicrobial spectrum depending on the type of infected wound. The ideal treatment would be produced at a low cost, and reduce both likelihood of inducing bacterial resistance, and toxicity to host tissue. The new agent would have persistent or residual skin activity to allow for infrequent dosing, stability in the presence of the physiologically relevant wound environment, and some local skin penetration but no systemic absorption. With these

considerations in mind, surface-tethered antimicrobial peptides (AMPs) are among the most promising technologies as alternative antimicrobials.

Antimicrobial Peptides (AMPs) and Human Cathelicidin LL37

AMPs naturally derived, short, cationic peptides found in the innate immunity of many species. They are broadly active against many different types of bacteria relevant to the chronic wound environment and their unique mechanisms do not allow significant resistance to develop. They are among the most attractive alternatives to antibiotics because they evoke immune response to react against infection (Gabriel, Nazmi, Veerman, Nieuw Amerongen, & Zentner, 2006). While many antibiotics utilize chemical mechanisms by specifically targeting cell surface biomarkers, AMPs physically penetrate the bacteria cell membranes, causing pores and eventual cell lysis. This physical versus chemical mechanistic difference makes AMPs more effective while making it more difficult for bacteria to develop resistance (Bagheri, Beyermann, & Dathe, 2008). Cathelicidins are a family of AMPs with a conserved N-terminal cathelicidin domain, and are part of the mammalian innate immune defense against invasive bacterial infection. The only human-derived cathelicidin is LL37, named for its 37 amino acid active domain beginning with two leucine residues, which is not only broadly antimicrobial but also has been shown to promote wound healing (Durr et al., 2006). The problem with clinical use of AMPs such as LL37; however, is that they are expensive to produce and may be cytotoxic in high concentrations.

The human cathelicidin peptide LL37, encoded by precursor hCAP-18 has shown potential in helping to treat infected chronic wounds because of its expression by epidermal keratinocytes and pro-healing functionality (Bourke et al., 2014). The full structure of LL37 contains an N-terminus signal sequence, a conserved cathelin-like domain, and an active C-

terminus. LL37 is expressed in the neutrophils and keratinocytes of inflamed skin has shown promotion of wound healing at concentrations of 0.2 to 1 μM and a variety of other functions, summarized in Figure 8. Concentrations above 13 μM are toxic to cells and concentrations below 0.2 μM demonstrate little to no effect in helping to heal the wound (Duplantier & van Hoek, 2013).

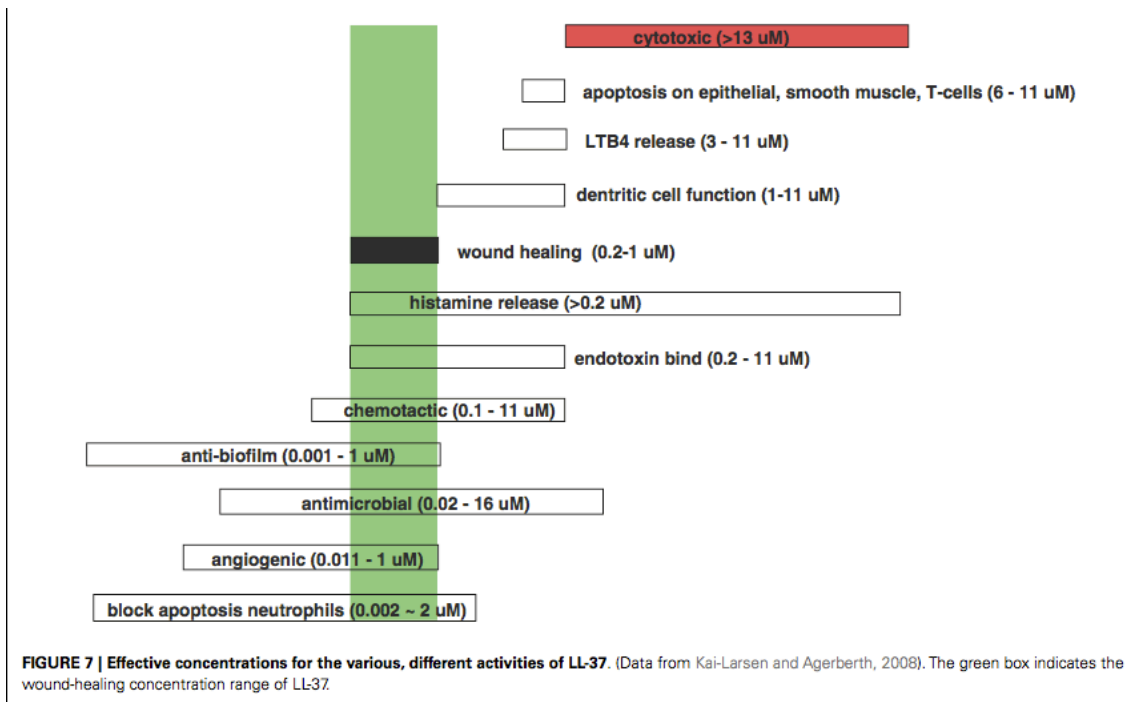


Figure 8: Different concentrations for the various activities of LL37 (Duplantier & van Hoek, 2013).

This toxicity has limited LL37 to topical applications, but there is still considerable interest in utilizing AMPs for systemic applications, where they will be most effective.

Lowering LL37 toxicity could allow to the therapeutic development of LL37 to treat chronic infected wounds (Duplantier & van Hoek, 2013). One of the most promising solutions to using AMPs is to covalently or non-covalently attach them to surfaces by developing a coating to reduce the possibility of bacterial infection (Onaizi & Leong, 2010). Covalent coatings would be

promising for preventing biofilm formation on medical implant surfaces (Ivanov, Morrison, Cobb, Fahey, & Camesano, 2012). In the case of metallic surfaces, LL37 has been covalently tethered and has retained its activity, but this tethering may alter its ability to promote healing. LL37 tethering has been limited to metallic surfaces; its tethering to soft substrates such as collagen has not been studied in detail (Gabriel et al., 2006).

There have been studies done regarding the wound healing ability of LL37. One example was an *in vitro* wound-healing assay. This assay showed that LL37 promoted keratinocyte (HaCaT) migration on fibronectin at concentrations up to 500 ng/ml which is important because proliferation and migration of human keratinocytes are important characteristics of effective wound healing (Carretero et al., 2008). The cathelicidin induced an increase in the tyrosine phosphorylation of focal adhesion kinase, which relates to the level of human keratinocyte motility (Carretero et al., 2008). Another study conducted *in vivo* was done in diabetic mice to determine the wound-healing enhancement of LL37 using retrovirus-transduced HaCaT cells and HaCaT cells untreated. They found that in most of the LL37-treated wounds at days 3 to 6 post-wounding and improved percentage of re-epithelialization. At day 6, in most cases, the edges of the wounded cells, or “epithelial tongues,” had converged to completely cover the wound when LL37 was present and the control wounds with no LL37 still showed a gap (Carretero et al., 2008).

Modified Collagen-Binding LL37 Design

Previously recombinant forms of human cathelicidin LL37 fused to collagen-binding domains (CBDs) were designed. Two CBDs, *c*CBD (TKKTLRT) from collagenase and *f*CBD (CQDSETGTFY) from fibronectin, were chosen, and chimeric CBD-LL37 (Figure 9), was expressed in human lung carcinoma cells (H1299). The long term goal of producing CBD-LL37

is its incorporation into a cell-derived matrix scaffold made of collagen (Prifti, 2012). The CBD was added to the C-terminus of LL37, the end associated with higher hemolytic activity, in order to tether the peptide to the matrix (Prifti, 2012). In order to allow flexible anchorage of the AMP, to aid in purification, and to allow commercial antibody recognition, a FLAG-tag octapeptide was used as a spacer molecule between the active domain and the CBD (Prifti, 2012).

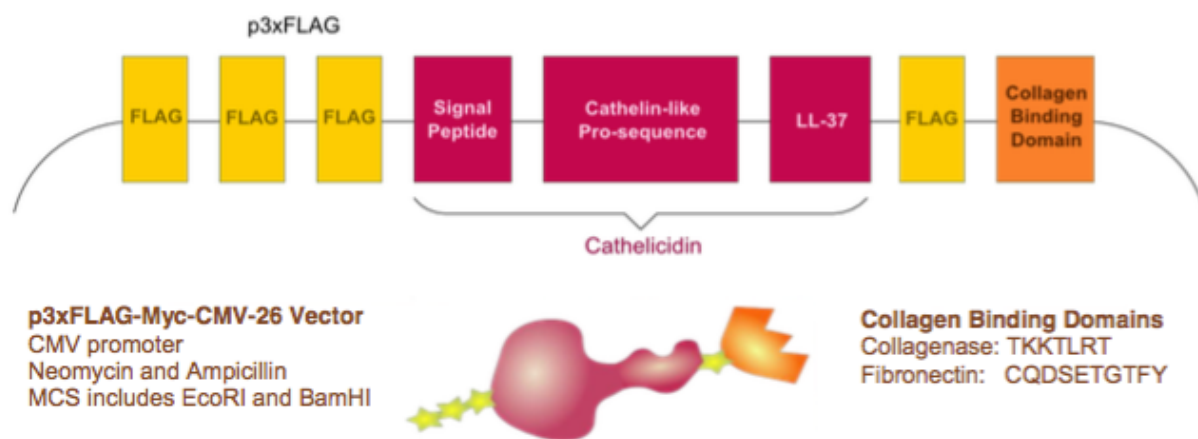


Figure 9: Full structure of *c*CBD-LL37 and *f*CBD-LL37 precursors taken from (Prifti, 2012). The AMP includes three FLAG domains and the cathelin-like signal and pro-sequences, all of which are cleaved after cellular secretion, leaving the LL37 active domain (red), one FLAG sequence as a spacer and identifiable sequence (yellow) and the collagen binding domain (orange).

Previously we have seen expected cleavage of the active domain after secretion and high antimicrobial activity of these recombinant peptides using Western blotting and antimicrobial assays. Also, we have seen antimicrobial stability up to 3 weeks, freeze-thaw cycles, and lyophilization, and preliminary biocompatibility, all in solution and not tethered. With this information, our goal was to study the wound healing activity of these new AMPs in solution based on results from a scratch assay.

Scratch Assay

Wound healing properties can be assessed using an *in vitro* scratch test assay by measuring cell migration into a breached area on a tissue-culture plate. Making a single scratch through a cell monolayer simulates this breach. The cells will move toward the opening in order to close the scratch. Cells migrate to re-establish cell-cell contacts. In order to analyze the migration, images are taken of the scratched area at different time intervals until the wound is closed as shown in Figure 10.

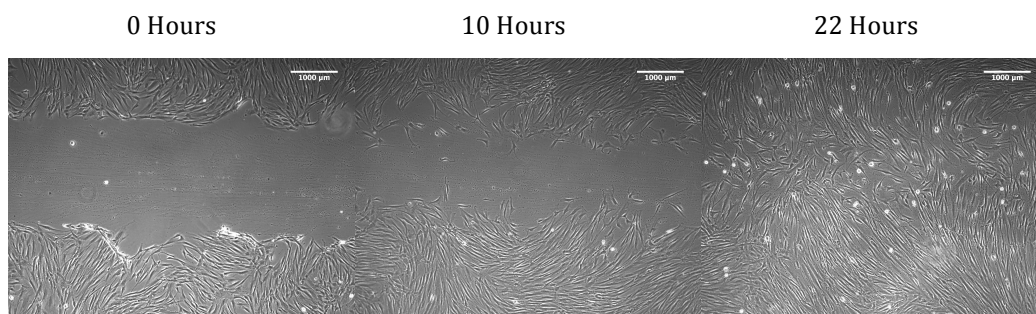


Figure 10: Example of scratch assay images of CT1005 fibroblasts at time points of 0 hours, 10 hours, and 22 hours, showing gap closure and healing.

An analysis was performed on the images taken by measuring the distance across the scratch. To find gap width, lines were drawn across the scratch at a 90-degree angle and analyzed using image analysis software. This distance becomes smaller over time if migration is occurring (Liang, Park, & Guan, 2007). By conducting scratch assays with CT 1005 fibroblasts exposed to synthetic LL37, synthetic *c*CBD-LL37 and both recombinant *c*CBD-LL37 and *f*CBD-LL37, we were able to study the ability of modified CBD-LL37 to promote wound healing versus unmodified LL37.

Materials and Methods

Materials

The following lists materials used for the scratch assay and basic cell culture equipment that was used as well as the manufacturers where each was purchased.

Dulbecco's Modified Eagle Medium (DMEM) and Ham's F-12 (Hyclone Media)
Fetal Bovine Serum (FBS) (Corning CellGro)
Dulbecco's Phosphate-Buffered Saline (DPBS) (Corning CellGro)
Glutamine (TCI)
Trypsin-EDTA (0.25%) (Corning CellGro)
10-cm dish (VWR)
6-well plate (Genesee Scientific)
CT 1005 Fibroblast Cells (Kindly donated by Dr. Tanja Dominko, WPI)
Synthetic peptides (*c*CBD-LL37 (New England Peptide, Gardner MA) and LL37 (Anaspec Inc., Fremont, CA)
Hemocytometer (VWR)
Zeiss Microscope (Kindly allowed permission to use by Sakthikumar Ambady)
Recombinant derived *c*CBD-LL37, *f*CBD-LL37, and wild-type (WT) conditioned media (Provided by Dr. Denis Kole)

Cell Culture Methods

When the cultured cells reached 70% confluence they were passaged. This was done by, first, aspirating the medium in the flask. Next, 5-mL of Dulbecco's Phosphate Buffered Saline (DPBS) was added and aspirated to remove dead cells and other debris. Trypsin was then added and the flask was rocked gently. Five mL of 1:1 Dulbecco's modified eagle medium/Ham's F-12 medium supplemented with 2.50-mM L-glutamine and 10% v/v fetal bovine serum (FBS) was added and mixed by pipetting up and down. The cells were then transferred to a 15-mL conical tube and centrifuged (Sorvall ST 8 Centrifuge, ThermoFisher, Waltham, MA) at 100 x g for 5 minutes. The supernatant medium was then aspirated and the cell pellet was re-suspended in 2-mL of media. The cells were pipetted up and down and a cell count was performed with a hemocytometer utilizing 10-uL of the cell solution. Once 2 cell counts were collected they were averaged and the number of cells per milliliter was calculated using chamber and cell solution

volumes. To determine the total number of cells remaining in the 15-mL conical, the cell volume used for the cell count was subtracted from the final value. The proper volume of cell suspension to be plated was determined by selecting the number of cells to be plated and then multiplying by the amount of media used to re-suspend the pellet and dividing by the number of cells in the 15-mL conical that was previously calculated. The cell suspension was then re-suspended and media was brought up to the proper final volume based on the dish on which the cells were plated. The cells were then placed in the incubator under humid conditions and 5.2% CO₂ at 37°C. Cells were checked for confluency and morphology every 24 hours. Media was aspirated, DPBS-rinsed, and replenished with 10-mL fresh media every 72 hours until ready to use in an experiment or to passage again at 70% confluence.

Preparing a Confluent Monolayer

Prior to starting the scratch assay, a confluent monolayer of cells was seeded onto a 6-well plate from cells growing on a 10-cm dish. A confluent monolayer is important for a scratch assay test to ensure that the cells grow in the scratched area only and do not grow on other areas of the plate. This is also representative of how cells would behave *in vivo*. Cells were passaged from the dish and plated on a 6-well plate with 135,000 cells per well. The growth area on a 6-well plate is 10-cm², meaning that a concentration of 13,500 cells per cm² could be used to plate cells on any well plate. The cells were then allowed to attach and grow for approximately 48 hours in order to develop a confluent monolayer. Each scratch assay had $n > 4$ replicates.

Baseline, (-)AMP Control

Once the cells had created a confluent monolayer, a sterile 200- μ L pipet tip was used to scratch the cells layer. Carefully holding the pipet tip straight up and down, each well of cells

was scratched once close to the center of the well. After the cells were scratched, their location was marked on the bottom of the plate and rinsed with DPBS to get rid of any dislodged or dead cells that would inhibit clear imaging. Finally, 2-mL fresh medium was added to each well and the cells were allowed to incubate. At chosen times of 0 hours, 4 hours, 10 hours, 15 hours, and 22 hours post-scratching, photos of each scratch were taken using a 5x objective lens on a Zeiss phase contrast microscope. Images were analyzed using ImageJ Analysis software, (<http://imagej.nih.gov/ij/>), using procedures described below in the data analysis section.

Sample, (+)AMP, Synthetic LL37 and cCBD-LL37 AMP

LL37 (Anaspec, Inc.) and cCBDLL37 (New England Peptide) AMPs were added into sample wells to determine (1) if adding AMP changed the closure time of the scratches compared to a (-) AMP control and (2) to determine if adding a cCBD moiety onto LL37 changed its ability to promote healing. This was done by adding AMPs directly from a 0.67-mM stock solution made in pH 7.4 PBS supplemented with 5-mM EDTA and 3-mg/mL BSA into the wells for final concentrations of 0.05- μ M, 3- μ M, and 12- μ M. AMPs were added directly after the DPBS rinse post-scratching and the final volume was brought up to 2-mL. All other methods were followed exactly and compared with the baseline control. Images were analyzed using ImageJ Analysis software.

Sample, (+)AMP, Recombinant cCBD-LL37 & fCBD-LL37

Serum-free conditioned medium (CM) from transfected H1299 (with both types of CBD-LL37, cCBD and fCBD) and untransfected H1299 (wild-type, WT) was collected after 90 hours in culture followed by overnight incubation in serum-free medium. CM was directly added onto the confluent monolayer of CT 1005 fibroblasts: 1-mL of CM from cCBD-LL37, fCBD-LL37, or

WT samples were added into 1-mL of medium into the well of a 6-well plate. The scratch assay proceeded as normal, with at $n > 4$ replicates. Images were analyzed using ImageJ Analysis software.

Imaging

Images were taken of the wound gaps as they healed over time with a Zeiss Microscope. The 5x objective lens was used on the microscope in order for the entire scratch to fit into one image. The images taken using the microscope at 0 hours, 4 hours, 10 hours, 15 hours and 22 hours showed that the scratches were closing because the scratch width decreased as time passed in the pictures taken.

Data Analysis

ImageJ software, (<http://imagej.nih.gov/ij/>), was used to analyze all images. For data analysis of the scratch width over time, each image was brought into ImageJ and the scale was set under the *analyze* tab. For each image the distance in pixels (picture height), the known distance, and unit of length were all set. The *global* setting was checked when the images had all the same dimensions. In order to set the “known distance” for the scale of the images the following equation was used:

$$\text{Known Distance in micrometers} = \frac{\text{image height} \times 10,000 \frac{\text{micrometers}}{\text{centimeter}}}{\frac{R}{2.54 \frac{\text{centimeters}}{\text{meter}}} \times M}$$

Where R was the picture pixels per inch that was found using image preview and M was the microscope eyepiece zoom (10x) multiplied by the objective lens (5x). Scale bars were drawn on each image taken of the scratch width tests over time.

Scratch Width Scratch Assay Results

Once the scale was set, 10, 90-degree, arbitrary lines were drawn across the scratch and were measured to determine the scratch width in μM as shown in Figure 11. A table summarizing all scratch width results can be found in Appendix B.

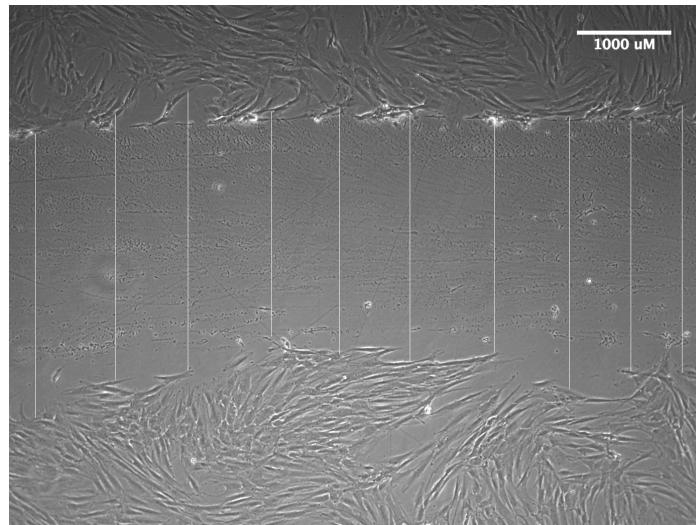


Figure 11: Representative image of the scratch width data analysis. This image is with $3 \mu\text{M}$ *c*CBD -LL37 at a time of 0 hours.

Percent Area of Wound

The percent area that the cells took up on the well over time was measured using a data analysis program written in ImageJ. This program analyzed the amount of free space on each image as it was imported into ImageJ and listed results as the amount of cells covering the plate in each image. The code developed to do this analysis and steps taken to collect the percent area can be found in Appendix C. This data was analyzed by first calculating the amount of space on each well that was not covered by cells because that was the area of the wound that needed to still heal and subtracting this value from 100 percent in order to compare the area still needed to heal to the scratch width results. A table summarizing the percent area results can be seen in Appendix B.

Wound Closure Rate: By Scratch Width and By Area

The wound closure rate was determined by graphing all averaged data points for scratch width (described in the *Scratch Width Scratch Assay Results* section) and percent area (described in the *Percent Area* section) over time. Then a linear trendline was applied to the points and the wound closure rate was found by the equation:

$$\text{Wound Closure Rate} = \frac{(\text{Normalized Scratch Width} - (y - \text{intercept}))}{\text{Time}}$$

The wound closure rate was found for all replicates for synthetic and recombinant cCBD-LL37, fCBD-LL37, and WT conditioned media, and then averaged together. Error was found using the standard error discussed below. A table summarizing the wound closure rate results is in Appendix B.

Error

Each scratch itself and image taken was unique, since the scratches were made by hand with a pipet tip and images were not done in exactly the same location on the plate at each time point; thus, error was relatively high. For all values, the **standard error** was used to analyze the data, calculated using the equation:

$$\text{Standard Error} = \frac{\text{Standard Deviation}}{n^{1/2}}$$

where n is the number of trials.

Normalization

Due to the original scratch width not being the same for every test the data was normalized in order to allow comparison of the results over time. The data was normalized so that the first point, at a time of 0 hours, was considered to be 100 percent, or the point with the

widest scratch. Each set of data was normalized to the original scratch width. To do this the average scratch width at each time point, including the first time point at 0 hours, was divided by the first average scratch width at 0 hours.

Propagated error was found when normalizing the data, since both of the numbers being divided had error. For the scratch width and percent area error the propagated error was calculated using the equation:

$$Propagated\ Error = Normalized\ Average * \sqrt{\frac{St.\ Dev.^2}{Avg} + \frac{Original\ St.\ Dev.^2}{Original\ Avg}}$$

where the “original” data used is the data to which the trial was normalized.

Statistical Significance

In order to determine if the data collected and results found were significant, a one-way analysis of variance (ANOVA) statistical test was used. The number of replicates for each condition is listed in Figure 12.

Sample	Replicates (n)
Control	25
0.05-μM cCBD -LL37	5
3-μM cCBD -LL37	4
12-μM cCBD -LL37	5
0.05-μM LL37	4
3-μM LL37	4
12-μM LL37	4
cCBD-LL37 CM	4
fCBD-LL37 CM	4
WT CM	4

Figure 12: Number of replicates analyzed for the scratch width, percent area, and wound closure rate. All samples were n > 4 with 25 control replicates.

In instances where statistical significance was found ($p < 0.050$), a post-hoc Tukey Test was used to locate the significance within the data set. One-way ANOVA on ranks tests were

performed on data sets where the equal variance condition could not be satisfied. All statistics were performed with SigmaPlot 12.5 software (Systat Software Inc., San Jose, CA).

Rationalizing Concentration Choice

The concentrations of synthetic, (+)AMP samples for LL37 and *c*CBD-LL37 were chosen to be 0.05- μ M, 3- μ M, and 12- μ M based on literature and our own biocompatibility investigations. We also performed preliminary MTT assays with our synthetic AMPs shown in Figure 13, which measure the ability of healthy fibroblasts to reduce MTT into formazan using visible spectroscopy. In short, CT 1005 fibroblasts were seeded on well plates at 4,000 cells/well and exposed to serial dilutions of AMPs between 0.01- μ M and 50- μ M. The resulting profile is similar to what has been reported in literature (Figure 8), demonstrating a wound healing effect between 0.5- μ M and 3- μ M, no effect on the rate of healing below 0.05- μ M, and toxicity above 10- μ M. Thus, we chose values within these three regimes.

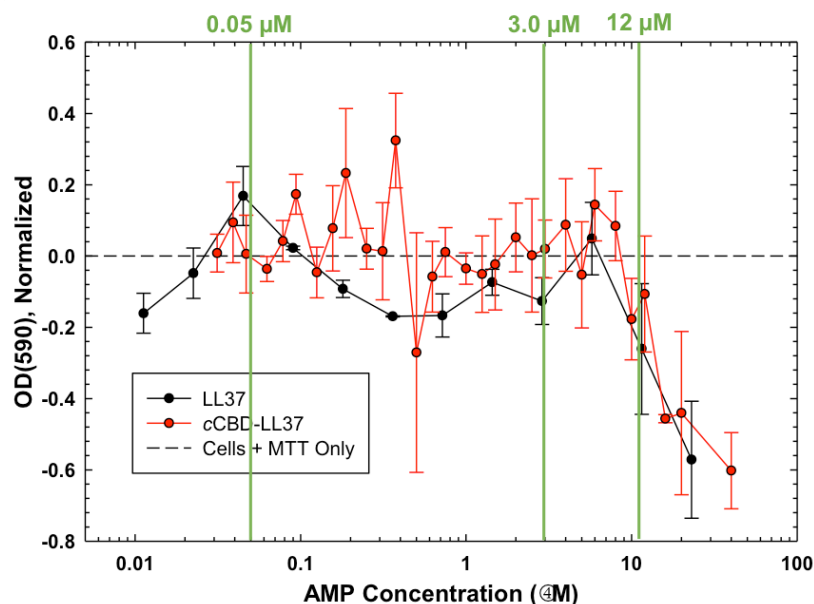


Figure 13: MTT Assay with CT Fibroblasts and both LL37 and *c*CBD-LL37. The error bars represent the standard deviation. All data was normalized to a no – AMP control as shown by the dotted line on the graph. Anything greater than this line was considered relatively “more proliferative” and anything below the line was relatively “less proliferative.” The AMP concentrations of 0.05- μ M, 3- μ M, and 12- μ M used for the experiments are also shown.

Results

Controls

For each scratch assay that was done a minimum of one control well with no AMP was also scratched. A representative panel of images demonstrating control well gap closure over time is presented in Figure 14. A total of $n > 24$ replicates were collected for the scratch width controls and percent area control that were averaged together and normalized. The normalized average of each control over time is plotted in Figure 15. The individual normalized scratch width, normalized percent area, and error calculations for each data set are summarized in Appendix B.

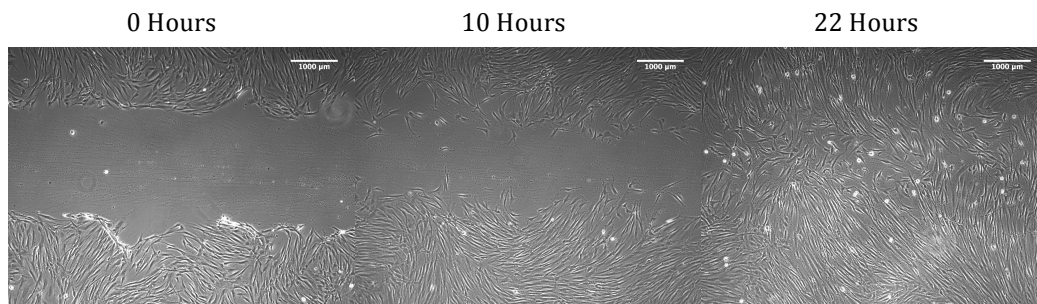


Figure 14: Control scratch images with no AMP at time points of 0 hours, 10 hours, and 22 hours during the scratch closure. Additional time points at 4 and 15 hours (not shown) were also taken for each experiment.

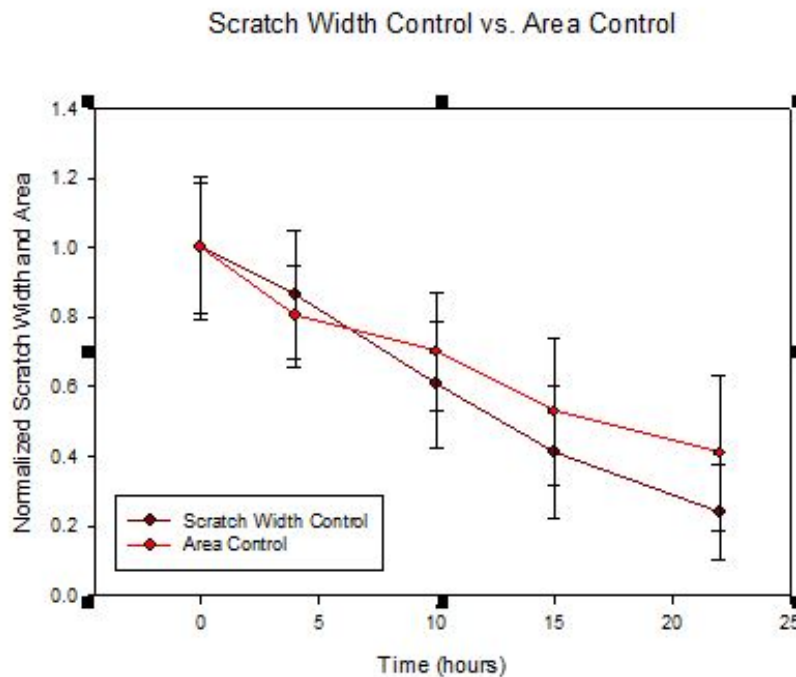


Figure 15: Overall normalized scratch width control versus overall normalized area to be closed over the time period of scratch closure. The error bars were found by calculating the propagated error at each time point. There was no statistical significance observed between the controls using one-way ANOVA, $p < 0.05$.

(+) Synthetic LL37 and cCBD-LL37 AMP Scratch Assay Results

Synthetic LL37 and cCBD-LL37 AMP were used at concentrations of 0.05- μ M, 3- μ M, and 12- μ M. A representative example of a scratch closing at different concentrations of cCBD-LL37 and LL37 over time is shown in Figure 16 and Figure 17, respectively.

***c*CBD-LL37 AMP**

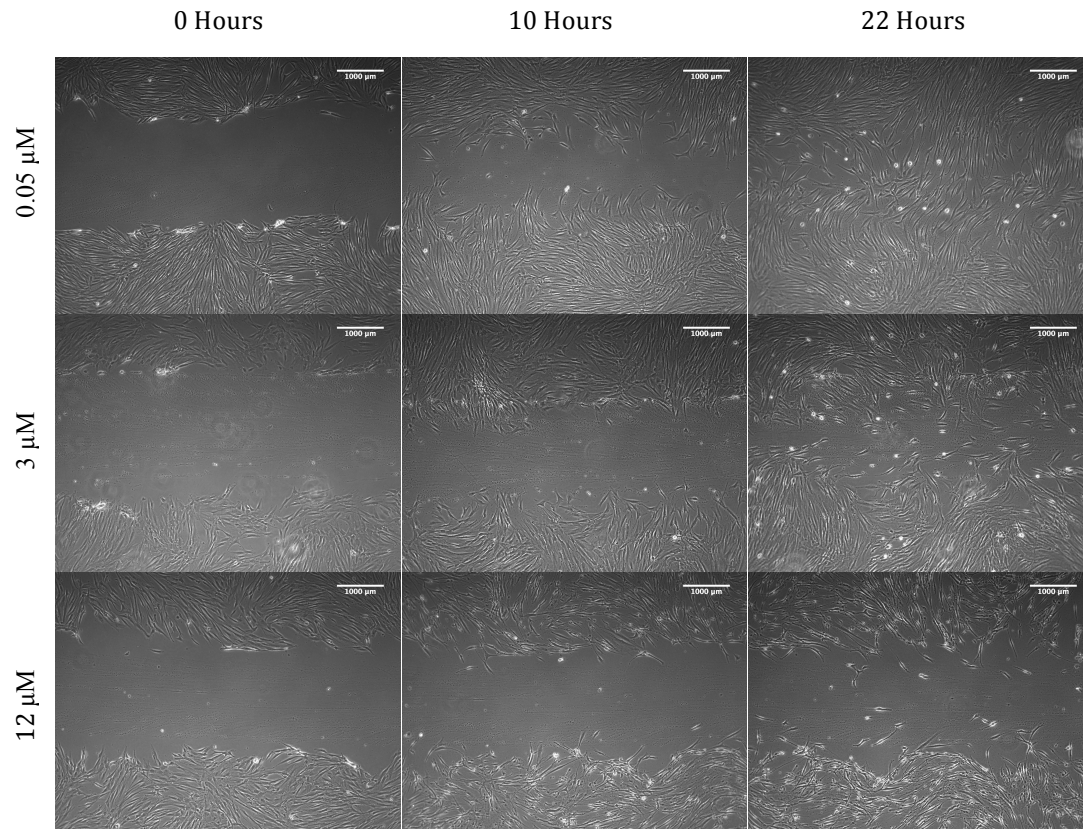


Figure 16: Three synthetic *c*CBD-LL37 AMP scratch images at concentrations of 0.05-μM, 3-μM, and 12-μM at time points of 0 hours, 10 hours, and 22 hours during the scratch closure. Additional time points at 4 and 15 hours (not shown) were taken for each experiment.

LL37 AMP

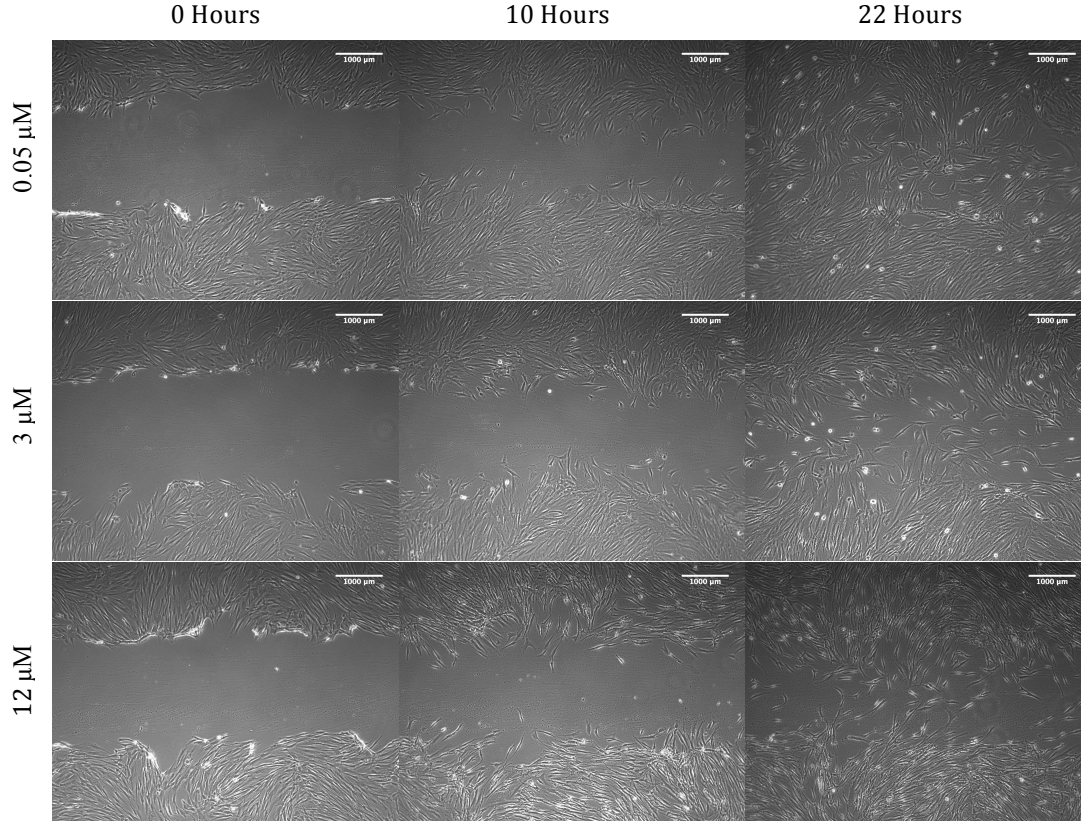


Figure 17: Three synthetic LL37 AMP scratch images at concentrations of 0.05- μM , 3- μM , and 12- μM at time points of 0 hours, 10 hours, and 22 hours during the scratch closure. Additional time points at 4 and 15 hours (not shown) were taken for each experiment.

The scratch width versus time for each AMP compared to the control is shown for 0.05- μM , 3- μM , and 12- μM concentrations in Figure 18, 19 and 20, respectively. Similarly, the exposed area percentage over time is demonstrated for each AMP at 0.05- μM , 3- μM , and 12- μM in Figure 21, 22, and 23, respectively. A minimum of $n = 4$ replicates were collected for each test and some had $n = 5$ replicates (Figure 12). All the trials collected and graphed were averaged together and normalized. The individual normalized scratch width, normalized percent area, and error calculations for each concentration are summarized in Appendix B.

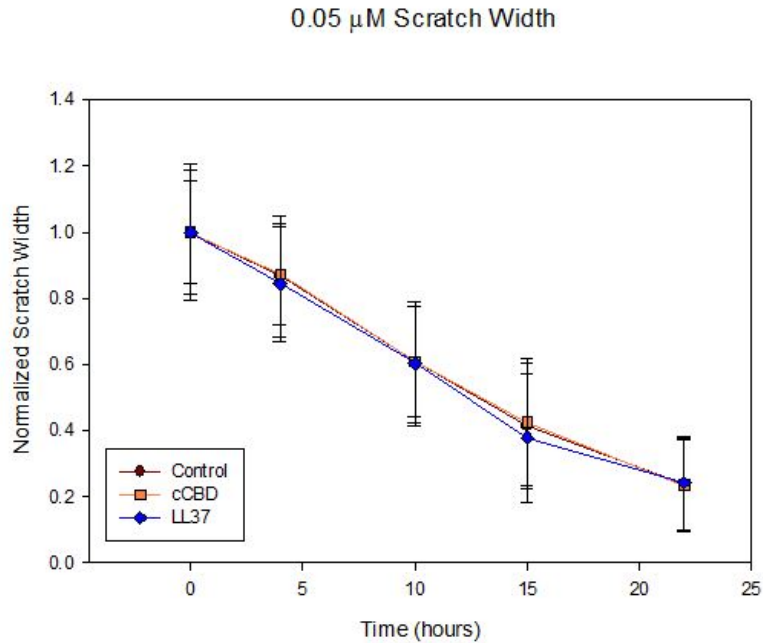


Figure 18: Overall normalized scratch width of 0.05- μ M AMP cCBD-LL37 and LL37 plotted against the overall average control measurements with no added peptide over the time period of scratch closure. The error bars were found by calculating the propagated error at each time point. There was no statistical significance ($p < 0.05$) seen for any time point.

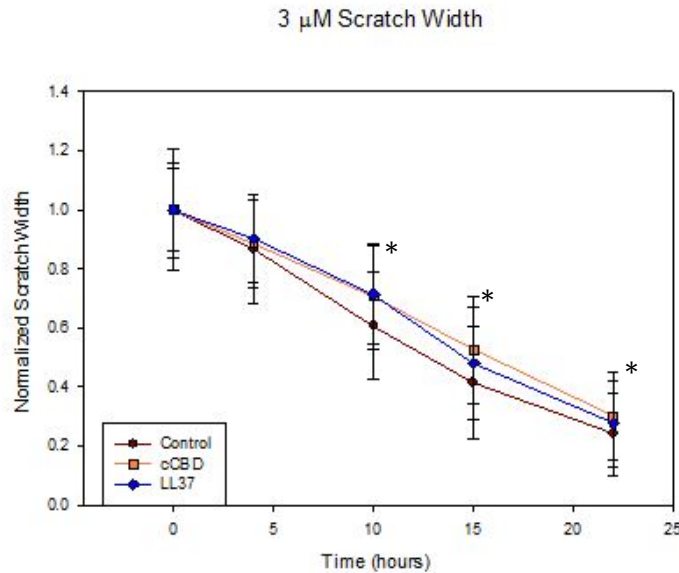


Figure 19: Overall normalized scratch width of 3- μ M AMP cCBD-LL37 and LL37 plotted against the overall average control measurements with no added peptide over the time period of scratch closure. The error bars were found by calculating the propagated error at each time point. (*) Indicates $p < 0.05$ at time points for cCBD-LL37 vs. other samples.

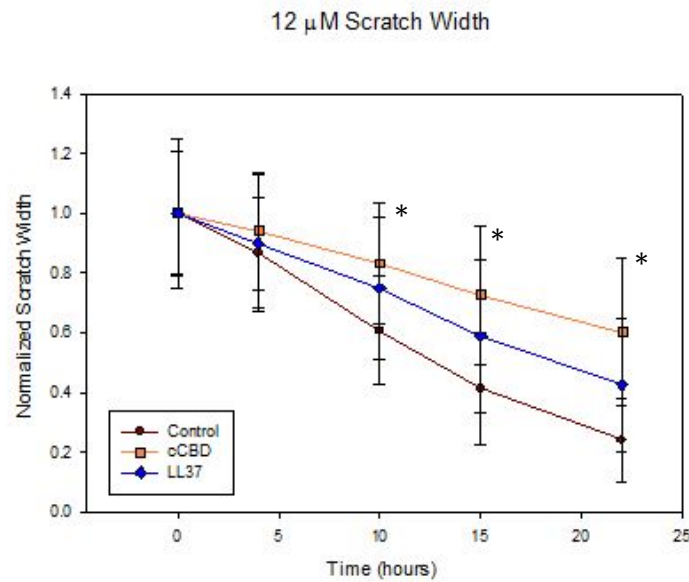


Figure 20: Overall normalized scratch width of 12- μ M AMP cCBD-LL37 and LL37 plotted against the overall average control measurements with no added peptide over the time period of scratch closure. The error bars were found by calculating the propagated error at each time point. (*) Indicates $p < 0.05$ at time points for cCBD-LL37 vs. other samples.

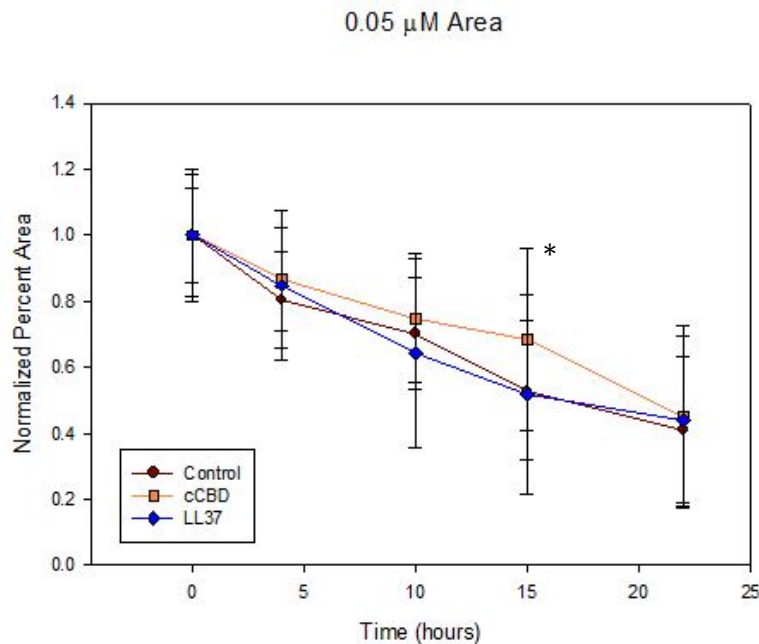


Figure 21: Overall normalized area still needed to be closed of 0.05- μ M AMP cCBD-LL37 and LL37 plotted against the overall average control measurements with no added peptide over the time period of closure. The error bars were found by calculating the propagated error at each time point. (*) Indicates $p < 0.05$ at time points for cCBD-LL37 vs. other samples.

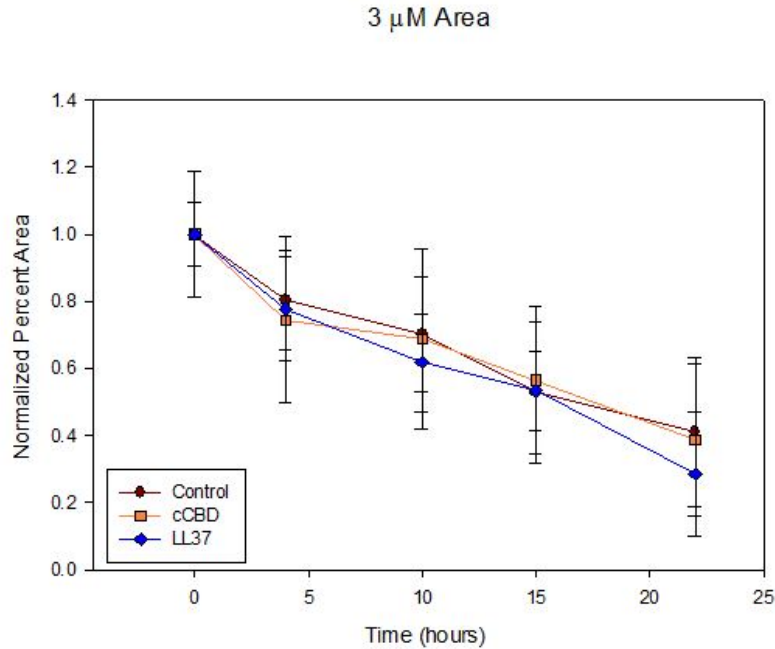


Figure 22: Overall normalized area still needed to be closed of 3- μ M AMP *c*CBD -LL37 and LL37 plotted against the overall average control measurements with no added peptide over the time period of closure. The error bars were found by calculating the propagated error at each time point. There was no statistical significance ($p < 0.05$) seen between any time points.

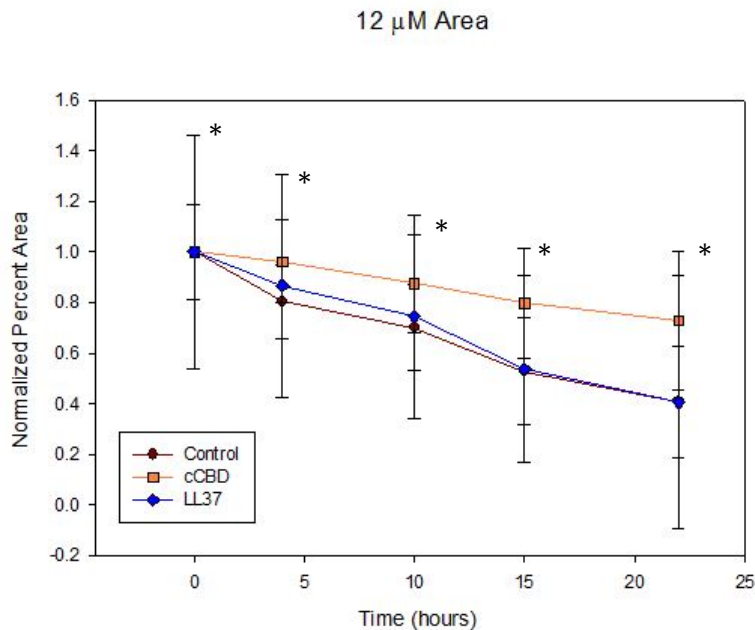


Figure 23: Overall normalized area still needed to be closed of 12- μ M AMP *c*CBD-LL37 and LL37 plotted against the overall average control measurements with no added peptide over the time period of closure. The error bars were found by calculating the propagated error at each time point. (*) Indicates $p < 0.05$ at time points for *c*CBD-LL37 vs. other samples.

Recombinant *cCBD-LL37* & *fCBD-LL37* and WT CM Scratch Assay Results

Similar to scratch assays with synthetic AMPs, a representative example of a scratch closing with *cCBD-LL37*, *fCBD-LL37*, and WT conditioned media is shown in Figure 24.

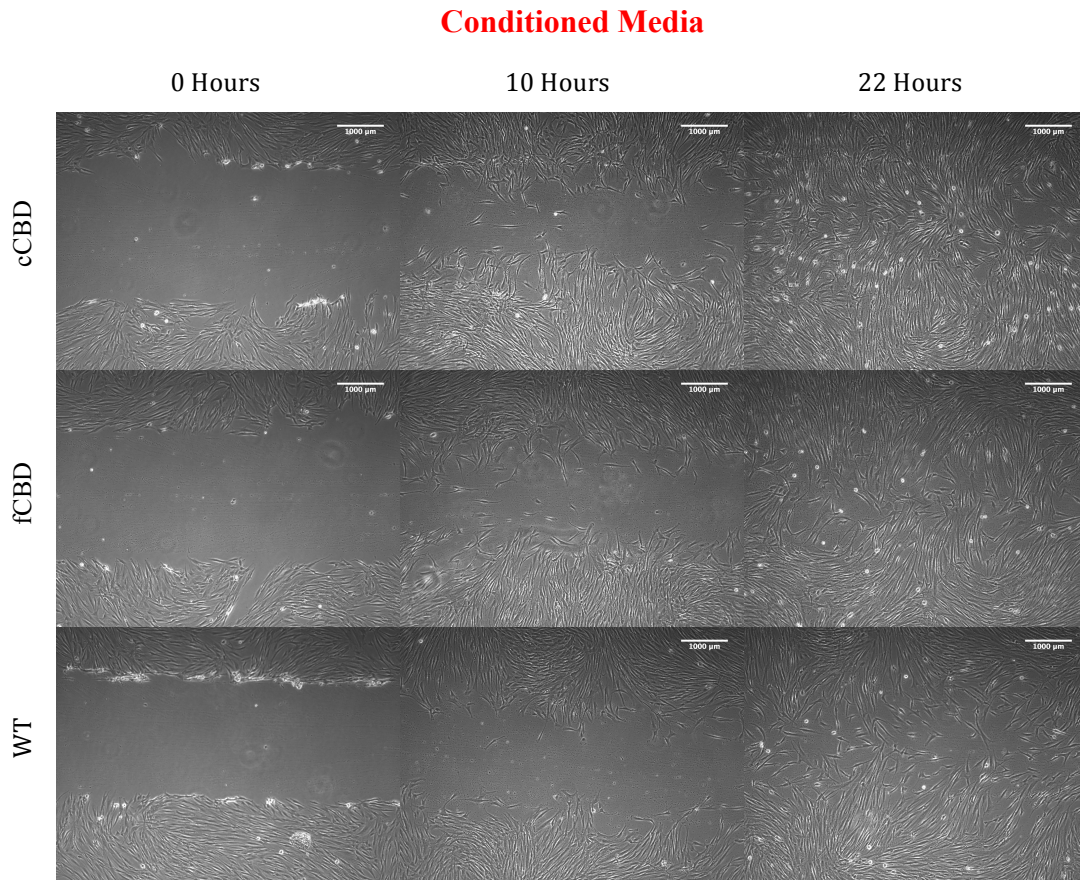


Figure 24: Different conditioned media used with CT 1005 cells during a scratch assay at time points of 0 hours, 10 hours, and 22 hours during the scratch closure. Additional time points at 4 and 15 hours (not shown) were taken for each experiment.

The scratch width data collected for recombinant CBD-LL37. *cCBD-LL37*, *fCBD-LL37*, and WT CM is graphed in Figure 25 and the exposed area percentage over time is demonstrated in Figure 26. A total of $n = 4$ replicates were conducted for each of the recombinant CBD-LL37. *cCBD-LL37*, *fCBD-LL37*, and WT CM media. The individual normalized scratch width, normalized percent area, and error calculations for each data set are summarized in Appendix B.

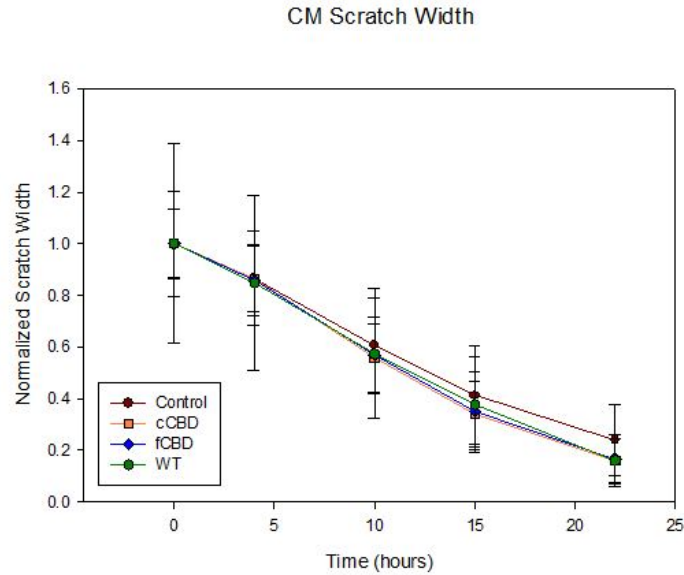


Figure 25: Recombinant cCBD-LL37 and fCBD-LL37 and WT CM normalized scratch width plotted against the overall average control measurements with no added conditioned media over the time period of scratch closure. The error bars were found by calculating the propagated error at each time point. There was no statistical significance ($p < 0.05$) seen between any data set.

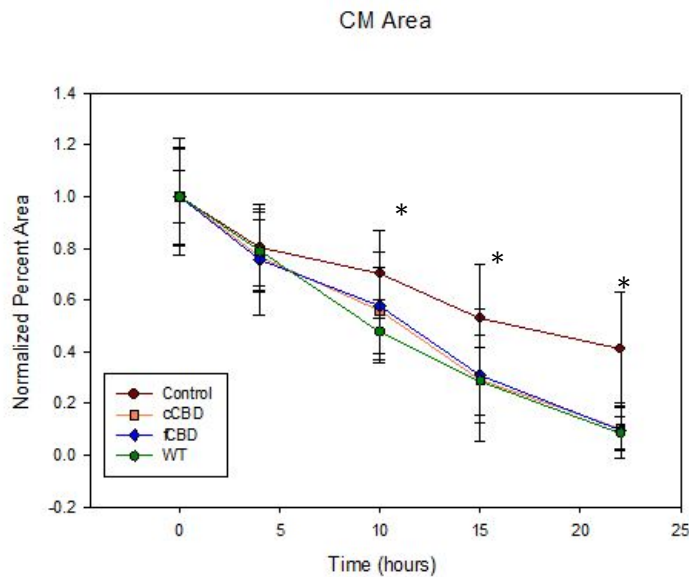


Figure 26: Overall normalized area still needed to be closed of recombinant cCBD -LL37 and fCBD-LL37 and WT CM plotted against the overall average control measurements with no added peptide over the time period of closure. The error bars were found by calculating the propagated error at each time point. (*) Indicates $p < 0.05$ at time points for cCBD-LL37 CM vs. other samples.

Wound Closure Rate

The wound closure rates determined for each sample analyzed using scratch width and analyzed using percent area are graphed below in Figures 27 and 28, respectively. All individual wound closure rates calculated and the error associated with each sample are summarized in Appendix B.

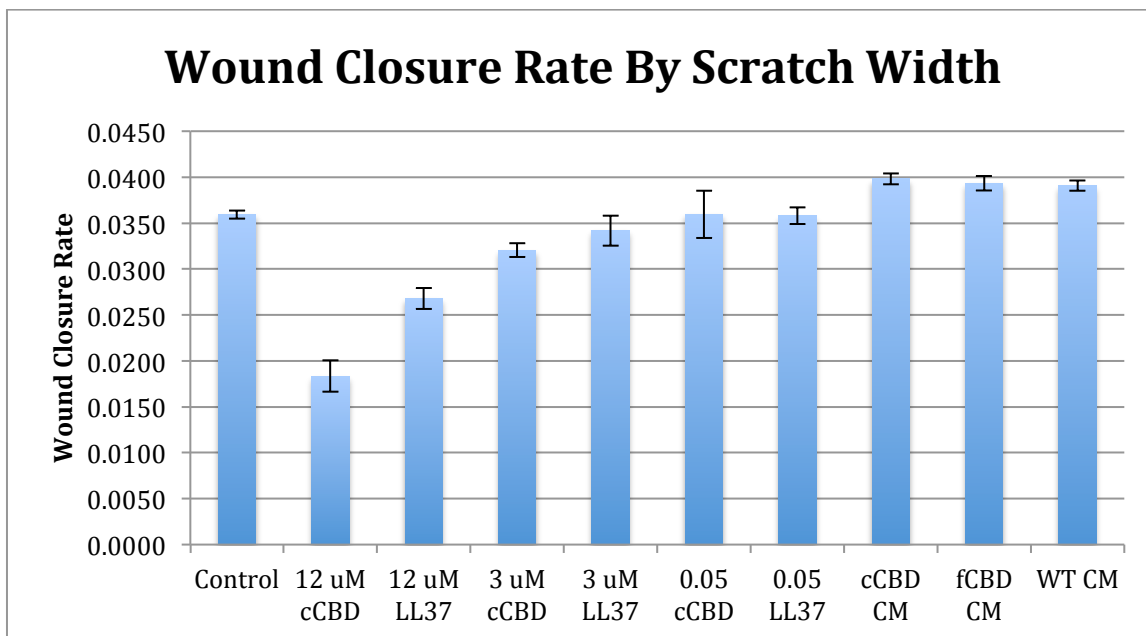


Figure 27a: Wound closure rate of the averaged scratch width over the 22-hour time period. The error bars were found by calculating the standard error of each test. Statistical analyses were performed using one-way ANOVA with $p < 0.05$. Statistical significance was observed and is described in Figure 26b, Figure 26c, and Figure 26d.

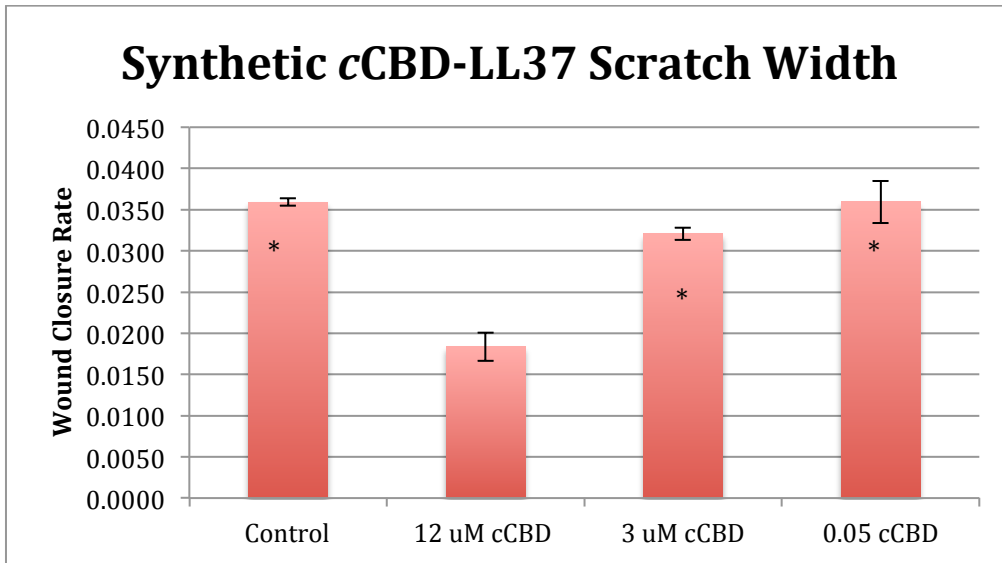


Figure 27b: Wound closure rate of the average scratch width of synthetic cCBD-LL37 vs. no AMP control over the 22-hour time period. (*) Indicates $p < 0.05$ for samples vs. 12- μ M cCBD - LL37.

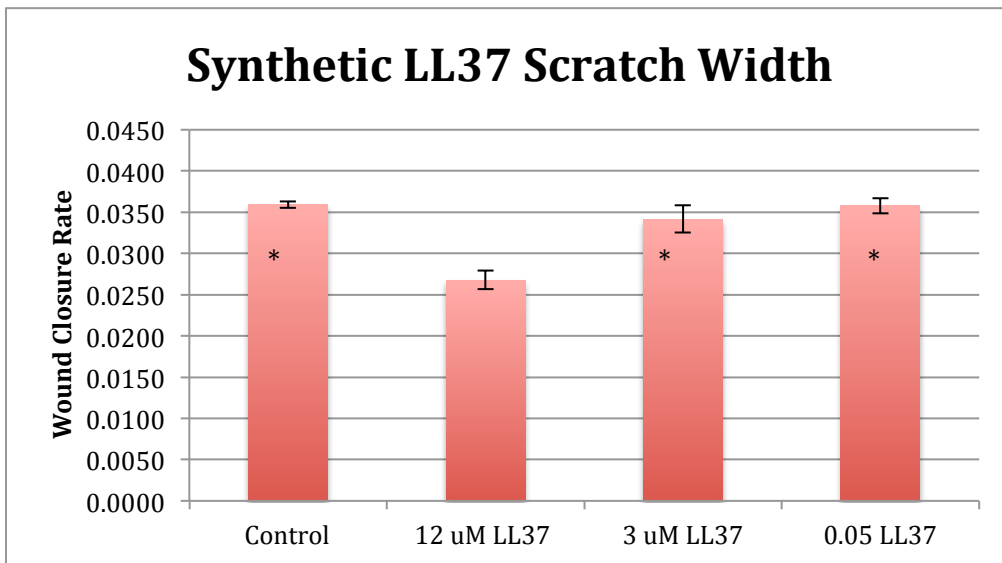


Figure 27c: Wound closure rate of the average scratch width of synthetic cCBD -LL37 vs. no AMP control over the 22-hour time period. (*) Indicates $p < 0.05$ for samples vs. 12- μ M LL37.

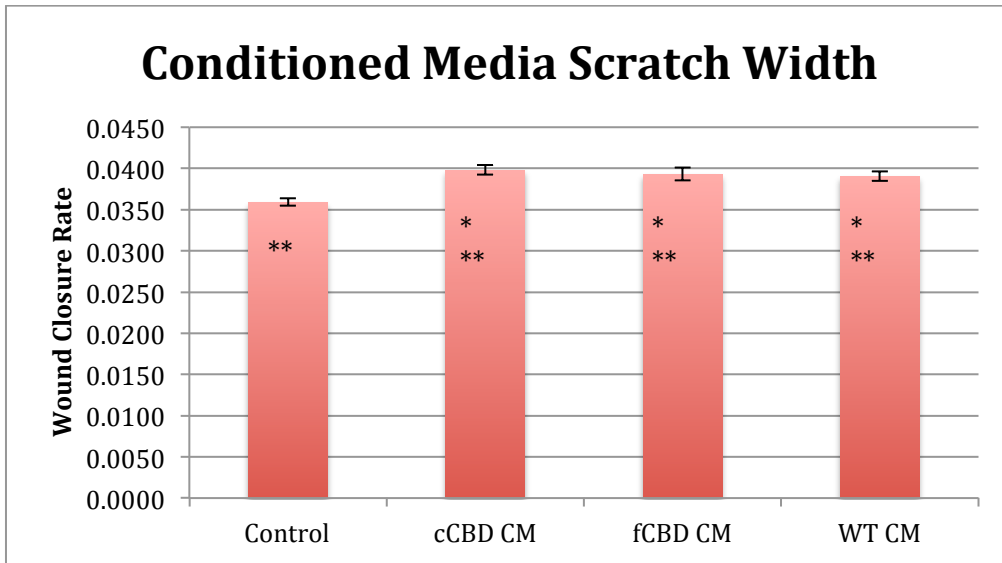


Figure 27d: Wound closure rate of the average scratch width of synthetic *c*CBD -LL37 vs. no AMP control over the 22-hour time period. The 3 conditioned media samples were not statistically significant compared to each other but were statistically significant compared to the no AMP control. (*) Indicates $p < 0.05$ for samples vs. 3- μ M *c*CBD -LL37. (**) Indicates $p < 0.05$ for samples vs. 12- μ M *c*CBD -LL37.

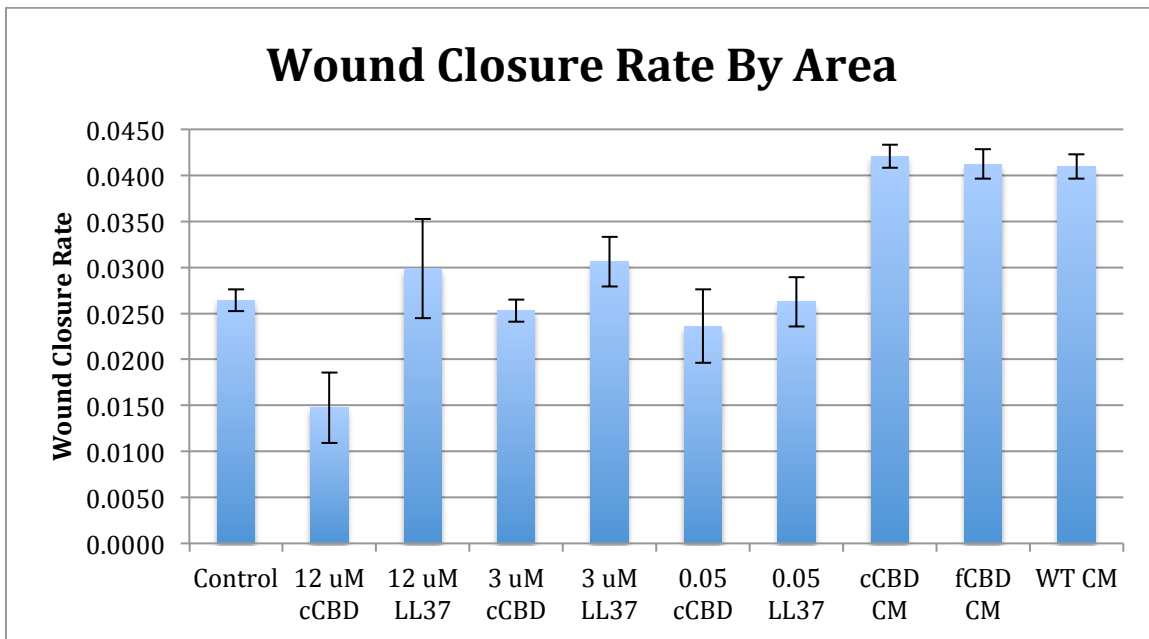


Figure 28a: Wound closure rate of the average percent area over the 22-hour time period. The error bars were found by calculating the standard error of each test. Statistical analyses were performed using one-way ANOVA with $p < 0.05$. Statistical significance was observed and is described in Fig. 27(b-d).

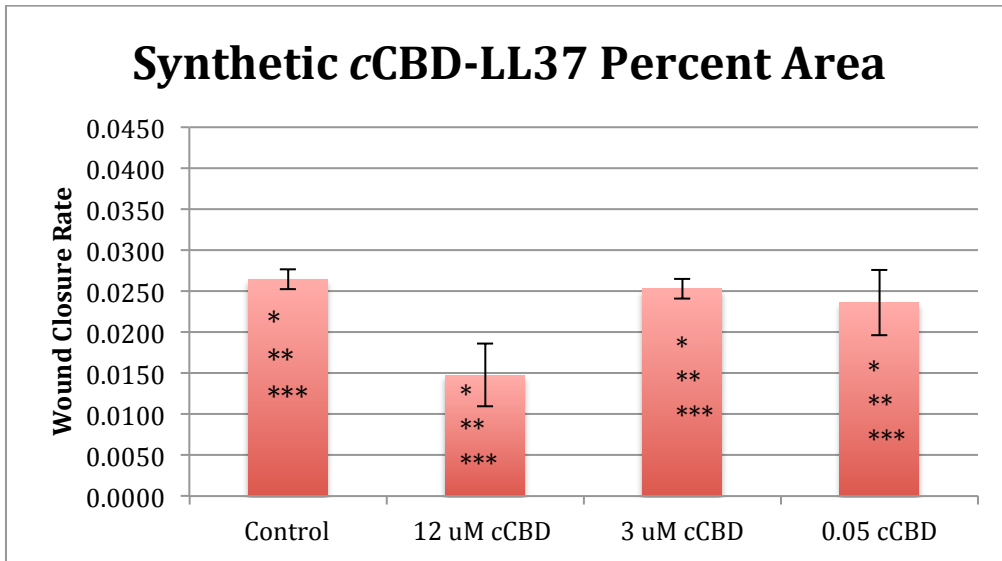


Figure 28b: Wound closure rate of the average percent area of synthetic *cCBD* -LL37 vs. no AMP control over the 22-hour time period. (*) Indicates $p < 0.05$ for samples vs. *cCBD*-LL37 CM. (**) Indicates $p < 0.05$ for samples vs. *fCBD*-LL37 CM. (***) Indicates $p < 0.05$ for samples vs. WT CM.

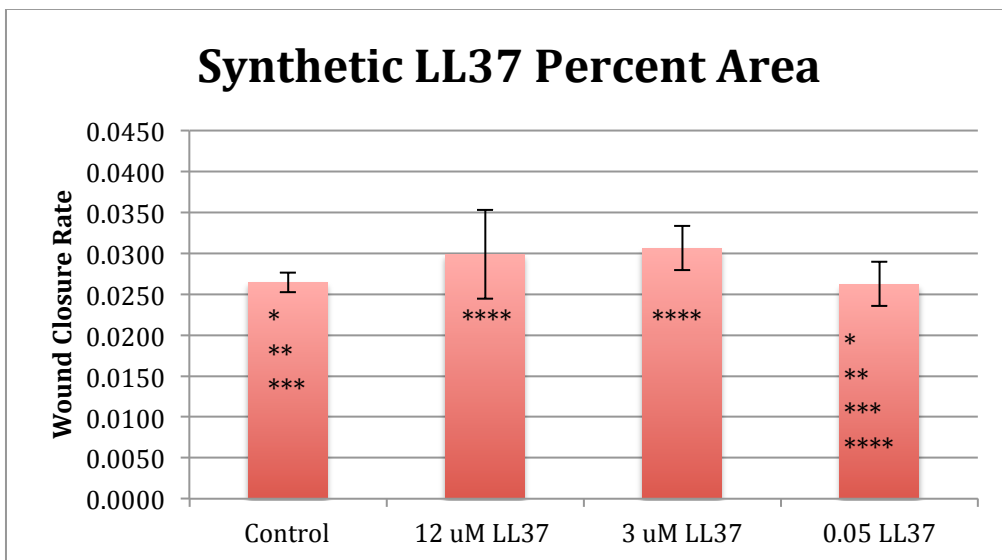


Figure 28c: Wound closure rate of the average percent area of synthetic LL37 vs. no AMP control over the 22-hour time period. (*) Indicates $p < 0.05$ for samples vs. *cCBD*-LL37 CM. (**) Indicates $p < 0.05$ for samples vs. *fCBD*-LL37 CM. (***) Indicates $p < 0.05$ for samples vs. WT CM. (****) Indicates $p < 0.05$ for samples vs. 12 μ M *cCBD* -LL37.

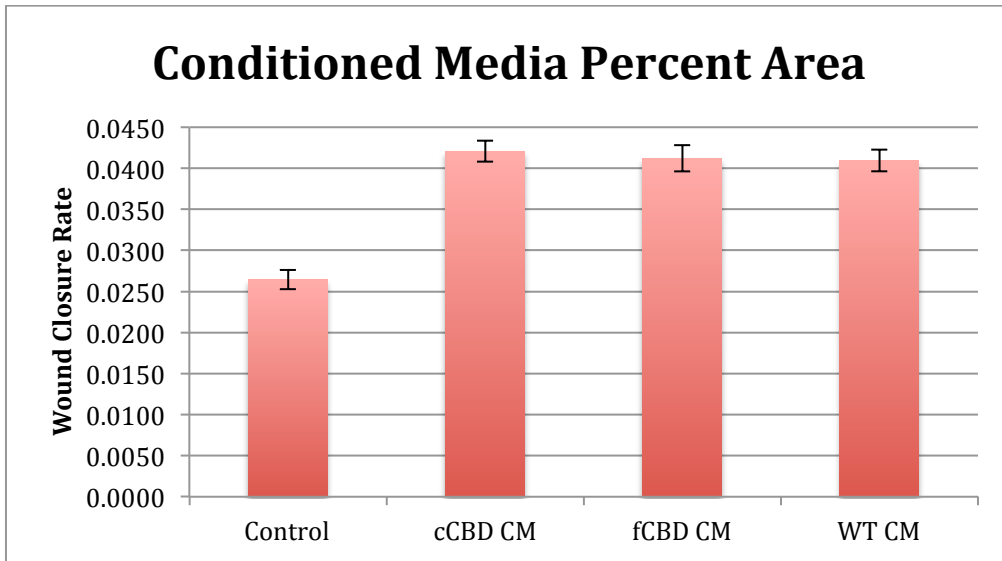


Figure 28d: Wound closure rate of the average percent area of conditioned media vs. no AMP control over the 22-hour time period. The 3 conditioned medias wound closure rates were not statistically significant from each other but all were statistically significant ($p < 0.05$) compared to the no AMP control.

Discussion

Controls

The average scratch width control over time and the percent area over time controls are not exactly the same as shown in Figure 15. Although these controls are not statistically significant different from one other, the area control appears to be slower in most cases. For both analyses the same images over time were used and the results were averaged together. The different result comes from the different methods of data analysis. For the scratch width analysis only 10 lines are drawn to measure the width while most studies that use this method draw approximately 100 lines per image. Although the 10 lines is a good representation of the scratch width, it is only an average of the precise scratch width. Most studies that use this method draw approximately 100 lines. The percent area was found using a computer program and the amount of area was calculated. There was no way to determine if each well had the exact same confluency, if any debris on the well affected the collected results, or if the program had inaccuracies due to the contrast seen in each individual image.

(+) Synthetic LL37 and cCBD-LL37 AMP Results

In general, it was observed that LL37 healed at a faster rate than cCBD -LL37 and any concentration of AMP used also healed at a slower rate than control. From the scratch width results in Figure 18, Figure 19, and Figure 20, at all concentrations the scratch width of cCBD -LL37 is larger than LL37 at each time point. Also from this data it was seen that both AMPs, no matter what concentration, healed at a slower rate than the no AMP control. For the percent area results in Figure 21, Figure 22, and Figure 23, there is a similar result that showed that cCBD -LL37 had more area to heal on the well at each time point than LL37 and both had more area to heal over time when compared to the no AMP control. This is one reason why the wound

closure rate analysis provided an alternative way to evaluate the data and validate scratch width and area findings.

The no AMP control healed at a faster rate than any concentration of *c*CBD-LL37 or LL37. This could be because the scratch assay was carried out *in vitro*. Proliferation and migration of keratinocytes are the most important aspects in wound healing and growth factors and cytokines have a significant influence upon these processes (Carretero et al., 2008). LL37 helps to promote wound healing by inducing chemotaxis of immune cells as well as dendritic cell differentiation and also induces the expression of chemokines and cytokines that help to heal wounds by activating (Carretero et al., 2008). Also, after the migration and proliferation of keratinocytes at the wound edge has started, proliferation of dermal fibroblasts in the area of the wound follows. The fibroblasts deposit large amounts of extracellular matrix and also help the wound contract to heal (Werner & Grose, 2003). One study looked into the different signals that are activated in order to help a wound heal. The expression of PDGF in the dermis and granulation tissue helped to heal a wound and studies done with diabetic mice had less PDGF that indicated that a certain expression level of PDGFs and their receptors as an essential part of normal wound repair (Werner & Grose, 2003). Since the study was conducted *in vitro* LL37 would not have been able to signal PDGF or other wound healing activities but a study could be done looking into the different wound healing signals and whether their absence from *in vitro* studies would inhibit wound healing. Without being able to signal the wound healing activities the addition of AMP may not speed up the wound healing process. Another wound healing study done *in vivo* on mice with recombinant and synthetic P-LL37 with a N-terminus analyzed the re-epithelialization of the wound. It was determined that the control wells keratinocyte layer was incomplete while the wounds treated with LL37 showed close to complete re-

epithelialization. This demonstrated that the healing process was accelerated when LL37 was used *in vivo* (Reinaldo et al., 2011). In the future it would be interesting to do a similar study *in vivo* to see if the same results would be achieved as seen in the previously described study.

The reasoning for observing slower migration in both the addition of AMPs in general vs. no AMPs and *c*CBD-LL37 vs. LL37 concentrations is likely similar. These results may be because *c*CBD-LL37 and LL37 have different structures. This different structure has been the cause of slightly higher antimicrobial activity observed previously by our group by *c*CBD-LL37. Since mechanisms against bacteria and mammalian cell membranes are related, higher activity by *c*CBD-LL37 could cause it to be more destructive toward fibroblast membranes thus causing slower healing. Also, LL37 has lower antimicrobial activity than *c*CBD-LL37 that could inhibit its wound closure rate, but both wounds would heal at a slower rate than the control (Wang, Nagarajan, & Camesano, 2014).

Another significant finding was that the 12- μ M concentration of both *c*CBD -LL37 and LL37 inhibited cell mobility and wound closure as shown in Figure 27b and Figure 28b. This is most likely because 12- μ M has been shown to be toxic to cells (Duplantier & van Hoek, 2013). A toxic concentration to cells can cause necrosis in which cells lose membrane integrity and die rapidly as a result of cell lysis, the cells can stop growing and dividing, or they can die (Usmani, 2011). This inhibited wound healing is apparent when compared to the 0.05- μ M and 3- μ M concentrations. Therefore, the 12- μ M concentration would not be used in an ECM scaffold due to its toxicity. In the future different tests could look into the molecular mechanisms behind LL37 versus bacterial membranes and mammalian membranes, the cell morphology changes with an increase in AMP concentration, or the mechanisms of cell death that could help explain the inhibited wound healing at the 12- μ M concentration.

Recombinant cCBD-LL37 & fCBD-LL37 and WT CM Results

From the scratch width results (Figure 18, Figure 19, and Figure 20), percent area results (Figure 21, Figure 22, and Figure 23), and wound closure rate results (Figure 27d and Figure 28d) it is evident that the *cCBD-LL37* CM, *fCBD-LL37* CM, and WT CM all healed at a faster rate than the no AMP control. The results show that something in the CM was influencing the cells growth in the scratch assays. Two possibilities of why they healed at a faster rate could have been due to something secreted by the cancer cells into the media or if the CT 1005 cells had been genotypically or phenotypically altered by the presence of H1299-conditioned medium. Further studies would need to be completed to determine the exact cause of these results.

Another notable observation was that there is no statistical significance seen between any of the different CM types. This was different than what we originally hypothesized. Since WT had no AMPs, we hypothesized that it would act like a control, no AMP well but there seemed to be something collected in this media that made it act like the *cCBD-LL37* and *fCBD-LL37* CM. This indicates that whatever is in the media is having a stronger effect on wound healing than the presence of AMPs and there could be very small concentrations of AMPs in the CM that are not affecting the wound closure rate.

In another study, it was found that the activity of mesenchymal stem cell (MSC) conditioned media played a role in skin wound closure by affecting both dermal fibroblast and keratinocyte migration, along with a contribution to the formation of extracellular matrix. It was also found that the enhanced wound closure rate was due to accelerated cell migration and not due to increased cell proliferation (Walter, Wright, Fuller, MacNeil, & Johnson, 2012). Although the conditioned media was taken from stem cells rather than cancer cells it could be possible they would act the same. Some future studies to look into would be to look into

whether the cells are proliferating and closing the gap or if they are actually closing the gap due to cell migration, determine the actual concentration of AMP within the conditioned media when 1-mL is used for a scratch assay, or the differences between the conditioned medias used and why they showed similar wound healing.

Wound Closure Rate

The wound closure rate was helpful to use in verifying the results seen with the scratch width and percent area analyses. Similar trends were observed for the wound closure rate graphs. This method would allow for the comparison of several different cell types, AMP types, and concentrations. The bar graph presentation of the wound closure rate also makes it easy to compare many data sets quickly. Finally, this method would allow for hundreds of data sets to be compiled and compared easily with any future scratch assays.

Sources of Error

The experiment had several areas where error could be introduced, but many replicates of each test were done to try and mitigate this error and the standard error was also used. In the experiment there was no way to make the starting scratch width the exact same for every test because they were scratched by hand so the data was normalized. Other problems that were encountered with the scratch assay and culturing cells can be found in Appendix D.

Overall Recommendations for ECM Incorporation of AMPs

One finding was that the results for any data analysis became more and more significant over time. This is because over time, wound healing becomes more apparent.

Before starting the scratch assays, we hypothesized that the addition of the *c*CBD moiety in the synthetic and recombinant *c*CBD-LL37 AMPs would not be significantly different than

unmodified LL37 at any of the concentrations. This was true for both AMPs at the 0.05- μ M and 3- μ M concentrations. At the 12- μ M concentration, there was a significant difference seen between the *c*CBD-LL37 and LL37 as well as the control. Since this concentration is toxic to cells and clearly inhibited wound closure, this concentration would not be used in an ECM scaffold. I also hypothesized that the highest migration rate of the CT 1005 cells would be observed at the middle concentration of 3- μ M because that was determined to be in the wound healing range for LL37. This was not shown by the results and overall when any concentration of AMP was added to the CT 1005 cells, wound closure was inhibited. This was most likely due to the fact that the scratch assay was carried out *in vitro* so it seems that many of the wound healing activities signaled by the AMP were not possible.

Conclusions

In order to develop a broad-spectrum chronic wound collagen dressing based on AMPs, several obstacles have to be overcome. One of the main drawbacks with almost all current antimicrobial treatments is the absence of broad-spectrum antimicrobial activity because over 200 species of bacteria can reside in a single chronic wound. Also, other obstacles with the use of AMPs for wound healing include toxicity, stability, and high manufacturing costs. We hypothesize that tethering AMPs onto collagen-based wound dressings will ultimately overcome these limitations by reducing toxicity (Onaizi, 2011), increasing AMP stability (Bagheri, 2009), and reducing costs by allowing a local therapeutic dosage of AMP to be delivered to a wound in the right concentration.

In this study the goal was to conduct scratch assay migration tests with synthetic *c*CBD-LL37, synthetic LL37, recombinant *c*CBD-LL37, recombinant *f*CBD-LL37, and WT CM, in solution and determine their ability to promote wound healing of CT 1005 fibroblasts *in vitro* over time at concentrations of 0.05- μ M, 3- μ M, and 12- μ M. Our original hypothesis was that the addition of the *c*CBD moiety in the synthetic and recombinant *c*CBD-LL37 AMPs would not be significantly different than unmodified LL37 at any of the concentrations. Of the concentrations tested, this proved to be true for the 0.05- μ M and 3- μ M concentrations. At the 12- μ M concentration there was a significant difference seen between the *c*CBD-LL37 and LL37 but this concentration was also toxic to the cells and would not be used in the future for an ECM scaffold. We also hypothesized that the highest migration of the fibroblasts would be observed at the middle concentration of 3- μ M based on literature suggestions and preliminary experimental results. On the contrary, the results presented here showed that any concentration of AMP added to CT 1005 cells inhibited wound healing. This was most likely due to the

scratch assay being carried out *in vitro*. A final major finding was that the CM healed at a faster rate than the no AMP controls and there was no statistical significance between each individual CM type. It is uncertain what exactly is making the wound heal faster with the addition of the CM but further tests studying cell proliferation versus cell migration, the composition of the conditioned media, and other tests would need to be conducted in order for this to be determined.

The next step of this study would be to evaluate migration of fibroblasts when exposed to CBD-LL37 tethered onto collagen at a fixed concentration. It has been suggested that tethering reduces toxicity of AMPs, so this suggests that the levels of toxicity, particularly at 12- μ M, would potentially reduce as a result of tethering and more migration might be seen. Also, it would be interesting to do tests to determine exactly what was making the conditioned media heal at a faster rate than the control and why the WT CM acted the same as the *c*CBD-LL37 and *f*CBD-LL37. Finally, in the future it might be worthwhile to do an *in vivo* scratch assay with AMPs to determine if there is a difference in the AMPs wound healing ability or do a chamber-based assay to study cell migration *in vitro*.

The long-term goal of this project is to tether AMPs to collagen-based chronic wound dressings using the CBDs in order to reduce AMP toxicity, improve AMP stability and strategically deliver a broadly-active antimicrobial agent to prevent chronic wound infection all while promoting healing. The results from this scratch assay will help show the need for a new approach in delivery modified CBD-LL37 via tethering and follow-up *in vivo* studies for commercial considerations, as well as to identify appropriate AMP delivery concentrations to choose for use in an ECM scaffold in the hopes of developing a new wound healing treatment.

References

- Bagheri, M., Beyermann, M., & Dathe, M. (2008). Immobilization Reduces the Activity of Surface-Bound Cationic Antimicrobial Peptides with No Influence upon the Activity Spectrum: American Society for Microbiology.
- Bourke, C., Prendergast, C., Sani, D., Oulton, T., Hall, R., & Mountford, A. (2014). Epidermal Keratinocytes Initiate Wound Healing and Pro-Inflammatory Immune Responses Following Percutaneous Schistosome Infection (Vol. 45, pp. 215-224): International Journal for Parasitology.
- Brett, D. (2008). A Review of Collagen and Collagen-based Wound Dressings (Vol. 20).
- Carretero, M., Escamez, M., Garcia, M., Duarte, B., Holguin, A., Retamosa, L., . . . Larcher, F. (2008). *In vitro* and *In vivo* Wound Healing-Promoting Activities of Human Cathelicidin LL-37 (Vol. 128, pp. 223-236): Journal of Investigative Dermatology.
- . Chronic Wound Care. (2015): Turven Health Analytics Inc.
- Dhandayuthapani, B., Yoshida, Y., Maekawa, T., & Kumar, S. (2011). Polymeric Scaffolds in Tissue Engineering Application: A Review. *International Journal of Polymer Science*, 2011, 19.
- . *Discharges of Inpatients from Nonfederal Hospitals*. (2010). Retrieved from http://www.cdc.gov/nchs/data/nhds/4procedures/2010pro4_numberprocedureag e.pdf.
- Dowd, S., Sun, Y., Secor, P., Rhoads, D., Wolcott, B., James, G., & Wolcott, R. (2008). Survey of bacterial diversity in chronic wounds using Pyrosequencing, DGGE, and full ribosome shotgun sequencing: BMC Microbiology.
- Duplantier, A. J., & van Hoek, M. L. (2013). The Human Cathelicidin Antimicrobial Peptide LL-37 as a Potential Treatment for Polymicrobial Infected Wounds. *Frontiers in Immunology*, 4(143), 14.
- Durr, U., Sudheendra, U., & Ramamoorthy, A. (2006). LL-37, the only human member of the cathelicidin family of antimicrobial peptides (Vol. 1758, pp. 1408-1425): Science Direct.
- . Essentials of Wound Healing. (2015). Wound Doc: Wound Care Solutions Telemedicine.
- Gabriel, M., Nazmi, K., Veerman, E. C., Nieuw Amerongen, A. V., & Zentner, A. (2006). Preparation of Ll-37-Grafted Titanium Surfaces with Bactericidal Activity (Vol. 17, pp. 548-550): Academic Centre for Dentistry Amsterdam.
- . Guideline for Disinfection and Sterilization in Healthcare Facilities. (2009): Centers for Disease Control and Prevention.
- Hyakusoku, H., Orgill, D., Teot, L., Pribaz, J., & Ogawa, R. (2010). Color Atlas of Burn Reconstructive Surgery.
- Ivanov, I., Morrison, A., Cobb, J., Fahey, C., & Camesano, T. (2012). Creating Antibacterial Surfaces with the Peptide Chrysopsin-1: Applied Materials & Interfaces.
- James, S. E., Booth, S., Gilbert, P., Jones, I., & Shevchenko, R. (2008). Strategies in Regenerative Medicine (pp. 1-33).
- Kim, H., Jang, J., Kim, S., & Cho, J. (2013). De Novo Generation of Short Antimicrobial Peptides with Enhanced Stability and Cell Specificity: PubMed.gov.

- Liang, C.-C., Park, A. Y., & Guan, J.-L. (2007). *In vitro* Scratch Assay: A Convenient and Inexpensive Method for Analysis of Cell Migration *in vitro* (Vol. 2, pp. 329-333): Nature Protocols.
- Lipsky, B. A., & Christopher, H. (2009). Topical Antimicrobial Therapy for Treating Chronic Wounds: Infectious Diseases Society of America.
- Onaizi, S. A., & Leong, S. (2010). Tethering Antimicrobial Peptides: Current Status and Potential Challenges (Vol. 29, pp. 67-74). *Biotechnology Advances*.
- Prifti, F. (2012). Fabrication of a Novel Matrix-Associating Antimicrobial Peptide for Enhanced Wound Healing.
- Regan, M. C., & Barbul, A. The Cellular Biology of Wound Healing.
- Reinaldo, R., Joao, S., Ana, R., Raquel, C., Luisa, G., Fernando, S., . . . Miguel, G. (2011). Wound Healing Activity of the Human Antimicrobial Peptide LL37: ScienceDirect.
- Sen, C. K., Gordillo, G. M., Roy, S., Kirsner, R., Lambert, L., Hunt, T. K., . . . Longaker, M. T. (2009). Human Skin Wounds: A Major and Snowballing Threat to Public Health and the Economy. *Wound Repair and Regeneration*, 17(6), 763-771. doi: 10.1111/j.1524-475X.2009.00543.x
- Shai, A., & Maibach, H. (2005). Wound Healing and Ulcers of the Skin.
- Usmani, M. (2011). What is cytotoxicity? : Research gate.
- Walter, M., Wright, K., Fuller, H., MacNeil, S., & Johnson, W. (2012). Mesenchymal stem cell-conditioned media accelerates skin wound healing: an in vitro study of fibroblast and keratinocyte scratch assays: PubMed.
- Wang, K., Nagarajan, R., & Camesano, T. (2014). Antimicrobial Peptide Alamethicin Insertion into Lipid Bilayer: A QCM-D Exploration (Vol. 116, pp. 472-481): *Colloids and Surfaces B: Biointerfaces*.
- Werner, S., & Grose, R. (2003). Regulation of Wound Healing Growth Factors and Cytokines (Vol. 83, pp. 835-870): American Physiological Society.

Appendices

Appendix A: Background Figures

Advantages

- High and sustained concentration of antimicrobial at the site of infection
- Limited total amount of antimicrobial needed
- Limited potential for systemic absorption and toxicity
- Can use novel agents not available for systemic use
- May enable avoidance of using systemic antibiotics, thereby reducing development of antibiotic resistance
- Directs attention of both patient and providers to the wound
- Easily applied as outpatient, by patient or caregiver, potentially reducing the need for institutional care
- Often better adherence to treatment, especially for children

Disadvantages

- Few agents have been proven to be effective in clinical trials
- Minimal penetration limits use to open wounds without cellulitis or deep soft-tissue spread of infection
- Systemic absorption of some agents may occur if used on large wounds
- Some cause local hypersensitivity or contact dermatitis reactions
- May interfere with wound healing processes
- Possible alteration of normal cutaneous flora
- Difficult to accurately dose
- Frequent reapplications may be needed
- May be difficult to apply or esthetically unacceptable to some patients
- Can become contaminated during recurrent use of multidose container

Figure 5: Advantages and disadvantages of using topical antimicrobial therapies including creams and ointments (Lipsky & Christopher, 2009).

Product and formulations	Formulation(s)	Bacterial spectrum	Advantages	Disadvantages	Cost ^a	Indications ^b and comments
Acetic acid	0.25%, 0.5%, and 1% solutions	Bactericidal against most gram-positive and gram-negative organisms, including <i>Pseudomonas aeruginosa</i>	Inexpensive. Shown to eliminate <i>P. aeruginosa</i> colonization from burns	Cytotoxic in vitro although maybe not in vivo; limited activity against biofilm	\$	No longer as widely used as it was in the past
Cadexomer iodine	Gel, ^c ointment, and dressing	Polysaccharide starch lattice; active agent is slowly released free iodine; broad spectrum of activity (same as iodine)	Reduced local toxicity compared to iodine; elemental iodine released on exposure to exudate	Application may cause stinging and erythema but less tissue damage than other iodine products; effect may not persist, and efficacy may be reduced in body fluids	\$\$	Indicated for use in cleaning wet ulcers and wounds and reducing microbial load in the wound environment
Cetrimide	Solution, 40%	Active against bacteria and fungi; not active against <i>P. aeruginosa</i>	May be less toxic to wound tissues than other antiseptics	May be corrosive and is potentially harmful if swallowed	...	Not available in the United States
Chlorhexidine gluconate	Solution, 2% and 4%; liquid, 2% and 4%; hand rinse, 0.5%; wipes, 0.5%; sponge/brush, 4%; and foam, 4%	Active against gram-positive bacteria (eg, <i>Staphylococcus aureus</i>) and gram-negative bacteria, including <i>P. aeruginosa</i>	Persistent activity up to 6 h after application; few adverse effects	Hypersensitivity, including anaphylaxis, generalized urticaria, bronchospasm, cough, dyspnea, wheezing, and malaise; may cause serious injury to the eye and middle ear; avoid contact with face or head; some resistance reported	\$	2% Chlorhexidine indicated as surgical hand scrub, hand wash, preoperative skin, skin wound cleanser, and skin cleaner; polyhexamide is a similar newer biguanide
Hexachlorophene	Liquid, 3%; foam, 0.23% with 56% alcohol	Biguanide that is bacteriostatic against <i>Staphylococcus</i> species and other gram-positive bacteria	May retain residual effect on skin for several days	Rapidly absorbed and may result in toxic blood levels; application to burns has resulted in neurotoxicity and death; may cause central nervous system stimulation and convulsions, dermatitis, and photosensitivity reactions	\$\$\$	Not recommended for routine use on wounds because of potential toxicity
Iodine compounds and iodine tincture ^a	Solution, 2% and 2.4%; and Nal strong iodine (Lugol's), 5% and 10% KI; for iodine tincture, 2% and 2.4% Nal with 47% alcohol, and 7%, 5% KI in 83% EtOH	Microbicidal against bacteria, fungi, viruses, spores, protozoa, and yeasts	Broad spectrum	Highly toxic if ingested or significantly absorbed; do not use with occlusive dressings; causes pain and stains skin and clothing; use cautiously in patients with thyroid disorders	\$	Iodine compounds are now rarely used for wound management; cadexomer iodine and povidone iodine products are less toxic
Povidone iodine ^a	Ointment, 1%, 4.7%, and 10%; solution, 1% and 10%; and wash, scrub, cleanser, gel, aerosol, gauze pad, swab, and others	Broad spectrum includes <i>S. aureus</i> and enterococci; active ingredient is liberated free iodine; shares spectrum but is less potent than iodine	Less irritating to skin and allergenic than iodine. Can be covered with dressings. Clinically significant resistance very rare	Antibacterial action requires at least 2 min contact; may cause stinging and erythema; effect may not persist, and efficacy may be reduced in body fluids; prolonged use may cause metabolic acidosis; stains skin and clothing; possible interaction with starches in dressings	\$	Indicated for perioperative skin cleansing and for cleansing and prevention of infection in superficial burns, incisions, and other superficial wounds
Sodium hypochlorite ^a (Dakin's solution and EUSOL)	Solution, 0.0125%, 0.125%, 0.25%, and 0.5%	Vegetative bacteria, viruses, and some spores and fungi	Inexpensive. No known systemic toxicity	May require prolonged contact for antibacterial action; inactivated by pus; toxic to fibroblasts and keratinocytes, and may cause pain or lyse blood clots	\$	Concentrations \leq 0.025% may be useful to reduce bioburden
Hydrogen peroxide ^c	Solution, 1% and 3%; and cream, 1%	Oxidizing agent active against many gram-positive and gram-negative bacteria	Broad-spectrum, bactericidal, inexpensive; no known resistance	May cause some discomfort	\$	Commonly used, but few clinical studies
Silver nitrate	Solution 0.5%, 10%, 25%, and 50%; ointment, 10%; and swabs, 25%–50%	Silver ions are bactericidal against a broad spectrum of gram-positive and gram-negative bacteria	Low cost; easily applied	Painful on application; stains tissues; may delay healing; concentrations $>$ 0.5% cause cauterization; inactivated by wound exudates and chlorine	\$	Although it was previously widely used, it has now been largely replaced by other compounds, including newer silver dressings
Silver dressings	At least 6 approved products with different properties	Slowly released silver ions have broad-spectrum, including MRSA and VRE	Provide sustained levels of active silver ions; microbial resistance is rare; less painful and few adverse effects than silver nitrate; variety of products adaptable to different types of wounds; infrequent application required	Levels of silver ions at wound interface not well defined; may cause silver staining of tissues; may delay epithelialization; relatively expensive; few published comparative trials	\$\$	Should not substitute for nonmedicated dressings for uninfected wounds; may be useful for subclinically infected, highly colonized wounds or for wounds being prepared for skin grafting

NOTE. EUSOL, Edinburgh University Solution of Lime; MRSA, methicillin-resistant *S. aureus*; VRE, vancomycin-resistant enterococci.

^a Costs are approximate in US\$ per day for treating 100-cm² wound, as follows: \$, $<$ \$3; \$\$, \$3–\$15; and \$\$\$, $>$ \$15.

^b US Food and Drug Administration–approved indications.

^c Available without prescription.

Figure 6: Several topical antimicrobial wound healing products and formulations currently available listed with advantages and disadvantages (Lipsky & Christopher, 2009).

- Properly targeted antimicrobial spectrum for the particular type of infected wound
- Rapid bactericidal activity
- Persistent or residual skin activity, allowing infrequent dosing
- Activity in the presence of body fluids and proteins in wound exudate
- Low likelihood of inducing bacterial resistance
- Some local skin penetration but no systemic absorption
- No associated toxic (to host tissue) or allergic reactions
- Acceptable cosmetic and aesthetic qualities
- Low cost

Figure 7: Several considerations and factors developed by clinicians and industry in order to develop the idea topical antimicrobial therapy (Lipsky & Christopher, 2009).

Appendix B: Scratch Width, Percent Area, and Wound Closure Rate Summarized Data

Scratch Width Results

Scratch Width All Controls (n = 25)					
Time Point	0 Hours	4 Hours	10 Hours	15 Hours	22 Hours
Average (µm)	2691.4144	2330.8705	1634.8421	1110.8032	645.9402
Normalized Average	1.0000	0.8660	0.6074	0.4127	0.2400
Standard Deviation	389.7490	362.3611	419.7691	422.4498	280.8504
Standard Error	14.2316	13.2316	15.3278	15.4257	10.2552
Propagated Error	0.2048	0.1840	0.1791	0.1680	0.1100

Scratch Width 0.05-µM cCBD (n = 5)					
Time Point	0 Hours	4 Hours	10 Hours	15 Hours	22 Hours
Average (µm)	2681.7887	2340.1191	1635.7559	1141.3511	631.0478
Normalized Average	1.0000	0.8726	0.6099	0.4256	0.2353
Standard Deviation	294.6066	316.9612	385.2706	437.1497	284.6632
Standard Error	24.0545	25.8798	31.4572	35.6931	23.2427
Propagated Error	0.1554	0.1522	0.1585	0.1696	0.1092

Scratch Width 0.05-µM LL37 (n = 4)					
Time Point	0 Hours	4 Hours	10 Hours	15 Hours	22 Hours
Average (µm)	2459.6303	2072.3135	1482.6088	931.4415	595.8637
Normalized Average	1.0000	0.8425	0.6028	0.3787	0.2423
Standard Deviation	327.6107	332.4127	398.8904	406.7564	232.4626
Standard Error	25.8999	26.2795	31.5351	32.1569	18.3778
Propagated Error	0.1884	0.1757	0.1810	0.1729	0.0999

Scratch Width 3-µM cCBD (n = 4)					
Time Point	0 Hours	4 Hours	10 Hours	15 Hours	22 Hours
Average (µm)	2831.3246	2506.1779	1998.0469	1486.9157	848.6870
Normalized Average	1.0000	0.8852	0.7057	0.5252	0.2997
Standard Deviation	321.4777	303.5605	439.5395	392.2482	359.2549
Standard Error	29.3468	27.7112	40.1243	35.8072	32.7953
Propagated Error	0.1606	0.1470	0.1747	0.1508	0.1314

Scratch Width 3-µM LL37 (n = 4)					
Time Point	0 Hours	4 Hours	10 Hours	15 Hours	22 Hours
Average (µm)	2679.0280	2418.3465	1910.6533	1284.2625	736.5164
Normalized Average	1.0000	0.9027	0.7132	0.4794	0.2749
Standard Deviation	261.8444	312.9655	371.6593	448.4365	289.7919
Standard Error	23.9030	28.5697	33.9277	40.9365	26.4543
Propagated Error	0.1382	0.1464	0.1553	0.1738	0.1115

Scratch Width 12-μM cCBD (n = 5)					
Time Point	0 Hours	4 Hours	10 Hours	15 Hours	22 Hours
Average (μm)	2483.1817	2334.7475	2065.6024	1803.2282	1490.1621
Normalized Average	1.0000	0.9402	0.8318	0.7262	0.6001
Standard Deviation	363.3890	348.3336	398.3944	456.5854	484.4088
Standard Error	29.6706	28.4413	32.5288	37.2800	39.5518
Propagated Error	0.2070	0.1965	0.2014	0.2124	0.2139
Scratch Width 12-μM LL37 (n = 4)					
Time Point	0 Hours	4 Hours	10 Hours	15 Hours	22 Hours
Average (μm)	2560.3286	2300.9731	1916.4780	1504.3373	1085.9351
Normalized Average	1.0000	0.8987	0.7485	0.5876	0.4241
Standard Deviation	454.8731	419.2356	501.3643	515.4977	430.1755
Standard Error	41.5240	38.2708	45.7681	47.0583	39.2695
Propagated Error	0.2513	0.2287	0.2367	0.2268	0.1841

Scratch Width cCBD CM (n = 4)					
Time Point	0 Hours	4 Hours	10 Hours	15 Hours	22 Hours
Average (μm)	2806.0110	2422.6658	1568.4900	954.9729	448.5060
Normalized Average	1.0000	0.8634	0.5590	0.3403	0.1598
Standard Deviation	269.6917	275.3082	327.8817	302.6230	196.6342
Standard Error	24.6194	25.1321	29.9314	27.6256	17.9502
Propagated Error	0.1359	0.1285	0.1286	0.1127	0.0717
Scratch Width fCBD CM (n = 4)					
Time Point	0 Hours	4 Hours	10 Hours	15 Hours	22 Hours
Average (μm)	2891.9010	2483.6071	1640.3616	1019.3522	482.4578
Normalized Average	1.0000	0.8588	0.5672	0.3525	0.1668
Standard Deviation	272.1240	318.4470	377.2553	373.2399	209.5497
Standard Error	24.8414	29.0701	34.4385	34.0720	19.1292
Propagated Error	0.1331	0.1366	0.1409	0.1333	0.0741
Scratch Width WT CM (n = 4)					
Time Point	0 Hours	4 Hours	10 Hours	15 Hours	22 Hours
Average (μm)	2609.2594	2212.1437	1499.4947	982.2413	414.8622
Normalized Average	1.0000	0.8478	0.5747	0.3764	0.1590
Standard Deviation	837.4636	749.9494	552.6582	401.6456	226.1670
Standard Error	76.4496	68.4607	50.4506	36.6651	20.6461
Propagated Error	0.4539	0.3958	0.2809	0.1957	0.1006

Percent Area Results

Percent Area All Controls (n = 25)					
Time Point	0 Hours	4 Hours	10 Hours	15 Hours	22 Hours
Average (μm)	46.9158	37.7140	32.9095	24.8215	19.2277
Normalized Average	1.0000	0.8039	0.7015	0.5291	0.4098
Standard Deviation	6.1737	4.7583	6.7802	8.5085	7.9625
Standard Error	0.7276	0.5608	0.7991	1.0027	0.9384
Propagated Error	0.1861	0.1465	0.1715	0.1943	0.1781

Percent Area 0.05-μM cCBD (n = 5)					
Time Point	0 Hours	4 Hours	10 Hours	15 Hours	22 Hours
Average (μm)	47.1950	40.8773	35.3149	32.2567	21.3162
Normalized Average	1.0000	0.8661	0.7483	0.6835	0.4517
Standard Deviation	4.8051	6.1712	7.5306	11.0436	10.7867
Standard Error	1.2407	1.5934	1.9444	2.8514	2.7851
Propagated Error	0.1440	0.1577	0.1768	0.2441	0.2331

Percent Area 0.05-μM LL37 (n = 4)					
Time Point	0 Hours	4 Hours	10 Hours	15 Hours	22 Hours
Average (μm)	42.6329	36.1496	27.4107	22.0085	18.6949
Normalized Average	1.0000	0.8479	0.6429	0.5162	0.4385
Standard Deviation	6.0188	8.1085	10.4940	9.7907	7.2446
Standard Error	1.5540	2.0936	2.7095	2.5280	1.8705
Propagated Error	0.1997	0.2247	0.2624	0.2409	0.1809

Percent Area 3-μM cCBD (n = 4)					
Time Point	0 Hours	4 Hours	10 Hours	15 Hours	22 Hours
Average (μm)	44.9917	33.4828	30.9117	25.3984	17.3332
Normalized Average	1.0000	0.7442	0.6871	0.5645	0.3853
Standard Deviation	2.9934	10.8875	6.6865	8.2801	8.5237
Standard Error	0.8641	3.1430	1.9302	2.3903	2.4606
Propagated Error	0.0941	0.2470	0.1555	0.1878	0.1912

Percent Area 3-μM LL37 (n = 4)					
Time Point	0 Hours	4 Hours	10 Hours	15 Hours	22 Hours
Average (μm)	47.8284	37.1988	29.5213	25.4964	13.6398
Normalized Average	1.0000	0.7778	0.6172	0.5331	0.2852
Standard Deviation	6.3253	5.4871	5.3917	3.2882	8.7107
Standard Error	1.8260	1.5840	1.5565	0.9492	2.5146
Propagated Error	0.1870	0.1541	0.1392	0.0985	0.1860

Percent Area 12-μM cCBD (n = 5)					
Time Point	0 Hours	4 Hours	10 Hours	15 Hours	22 Hours
Average (μm)	34.8532	33.5529	30.5033	27.7889	25.4281
Normalized Average	1.0000	0.9627	0.8752	0.7973	0.7296
Standard Deviation	4.6494	3.4241	5.9890	5.2541	8.1835
Standard Error	1.2005	0.8841	1.5463	1.3566	2.1130
Propagated Error	0.1887	0.1617	0.2077	0.1845	0.2542

Percent Area 12-μM LL37 (n = 4)					
Time Point	0 Hours	4 Hours	10 Hours	15 Hours	22 Hours
Average (μm)	34.5131	29.9307	25.6691	18.5429	14.0211
Normalized Average	1.0000	0.8672	0.7437	0.5373	0.4063
Standard Deviation	11.2706	11.6372	9.6207	10.7029	15.2807
Standard Error	2.9101	3.0047	2.4841	2.7635	3.9455
Propagated Error	0.4618	0.4403	0.3697	0.3563	0.4622

Percent Area cCBD CM (n = 4)					
Time Point	0 Hours	4 Hours	10 Hours	15 Hours	22 Hours
Average (μm)	47.5274	37.5277	22.7795	13.6673	4.0906
Normalized Average	1.0000	0.7896	0.4793	0.2876	0.0861
Standard Deviation	6.3708	5.0419	4.8423	5.4570	2.5720
Standard Error	1.8391	1.4555	1.3979	1.5753	0.7425
Propagated Error	0.1896	0.1499	0.1204	0.1211	0.0553

Percent Area fCBD CM (n = 4)					
Time Point	0 Hours	4 Hours	10 Hours	15 Hours	22 Hours
Average (μm)	44.7483	33.7918	25.7919	13.9301	4.2347
Normalized Average	1.0000	0.7552	0.5764	0.3113	0.0946
Standard Deviation	7.1402	7.9139	7.1538	10.8148	3.4502
Standard Error	2.0612	2.2845	2.0651	3.1220	0.9960
Propagated Error	0.2257	0.2140	0.1844	0.2467	0.0786

Percent Area WT CM (n = 4)					
Time Point	0 Hours	4 Hours	10 Hours	15 Hours	22 Hours
Average (μm)	41.8989	32.2766	23.4461	12.2856	4.2865
Normalized Average	1.0000	0.7703	0.5596	0.2932	0.1023
Standard Deviation	3.0389	5.4683	5.6792	6.4241	2.5946
Standard Error	0.8773	1.5786	1.6394	1.8545	0.7490
Propagated Error	0.1026	0.1420	0.1415	0.1548	0.0624

Wound Closure Rate Results

Scratch Width	Wound Closure Rate	Standard Error
12-μM cCBD	0.0183	0.0017
12-μM LL37	0.0268	0.0011
3-μM cCBD	0.0321	0.0007
3-μM LL37	0.0342	0.0016
0.05-μM cCBD	0.0359	0.0026
0.05-μM LL37	0.0358	0.0009
cCBD CM	0.0398	0.0006
fCBD CM	0.0393	0.0008
WT CM	0.0391	0.0006
Control	0.0359	0.0004

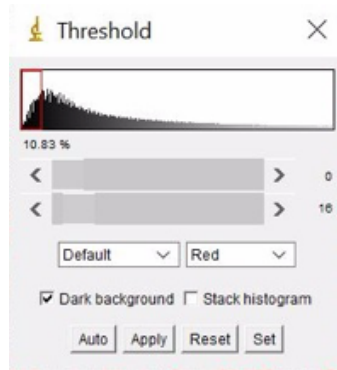
Percent Area	Wound Closure Rate	Standard Error
12-μM cCBD	0.0148	0.0038
12-μM LL37	0.0299	0.0054
3-μM cCBD	0.0253	0.0012
3-μM LL37	0.0306	0.0027
0.05-μM cCBD	0.0236	0.0040
0.05-μM LL37	0.0262	0.0027
cCBD CM	0.0421	0.0013
fCBD CM	0.0412	0.0016
WT CM	0.0410	0.0013
Control	0.0264	0.0012

Appendix C: ImageJ Program*

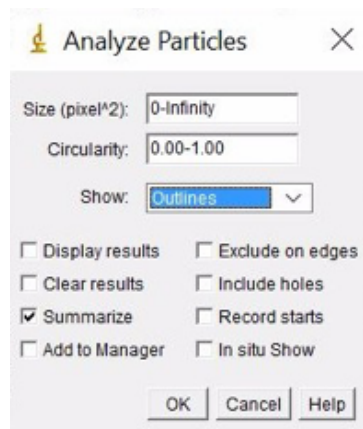
```
run("Images to Stack", "name=Stack title=[] use");
run("Find Edges", "stack");
run("Find Edges", "stack");
setAutoThreshold("Default dark");
//run("Threshold...");
setOption("BlackBackground", false);
run("Make Binary", "method=Default background=Default calculate black");
run("Fill Holes", "stack");
run("Analyze Particles...", "size=0-100000000 show=Outlines summarize stack"
```

The process to analyze a set of images and determine the percent area required many steps; (1) Stack the images to allow for bulk analysis (Image>stack>images to stack), (2) The

borders of the cells were found and this was done twice to create a better outline (Process>find edges), (3) The threshold function was used to reduce the impact of smudging and streaking in the analysis (Image>adjust>threshold>0/16>dark background>apply)



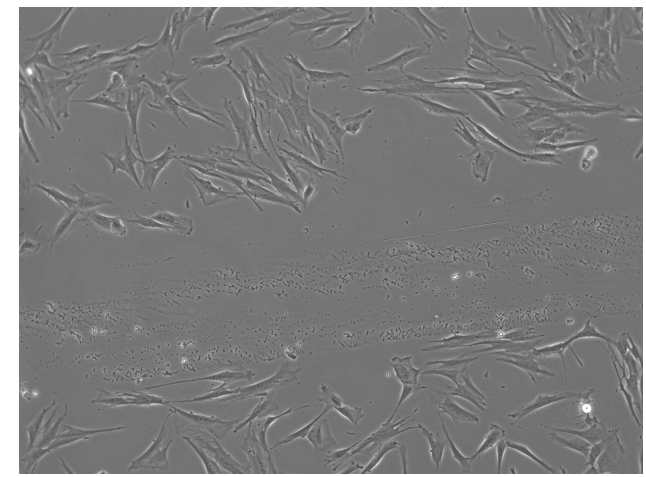
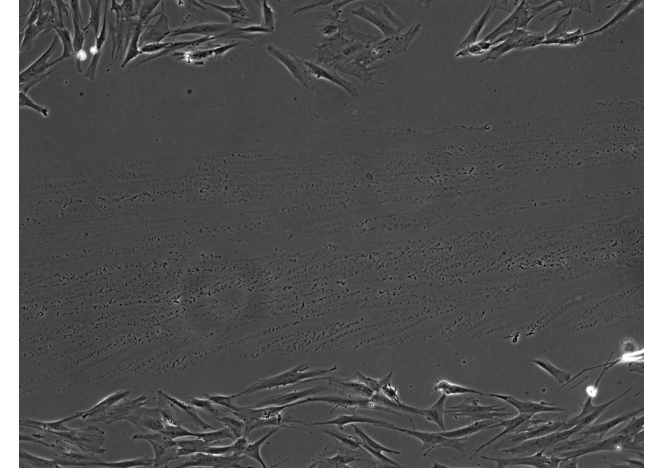
(4) The image was made binary to fill the holes in order to create an outline of the wound (Process>binary>make binary and Process>binary>fill holes), (5) A table of data for all the images was outputted which included percent area covered by cells (Analyze>analyze particles>size 0-infinity circularity 0-1>show outlines>summarize).



*Development of this program was completed with the help of Nick Bergstrom (WPI)

Appendix D: Troubleshooting Guide

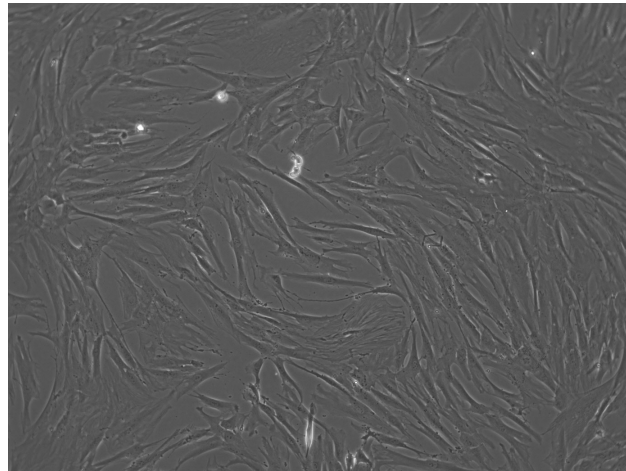
Culturing cells can be difficult and requires some trial and error. The following table shows some problems that could be encountered during this experiment and how to resolve these problems. Images are provided to show some examples.

Problem	<i>Resolution, Discussion and Example Images</i>	
Scratches are inconsistent	<i>Scratch at an angle (a) is more inconsistent</i> <i>Scratch with the pipet straight up and down (b)(90 degree normal to surface) is more consistent.</i>	<p data-bbox="714 504 1356 640">No peptide added to this image of a scratch taken at an approximate 45-degree angle like holding a pencil with a 5x objective lens and a 10x eyepiece on microscope.</p>  <p data-bbox="714 1165 1356 1270">No peptide added to this image of a scratch taken at a 90-degree angle with a 5x objective lens and 10x eyepiece on microscope.</p> 

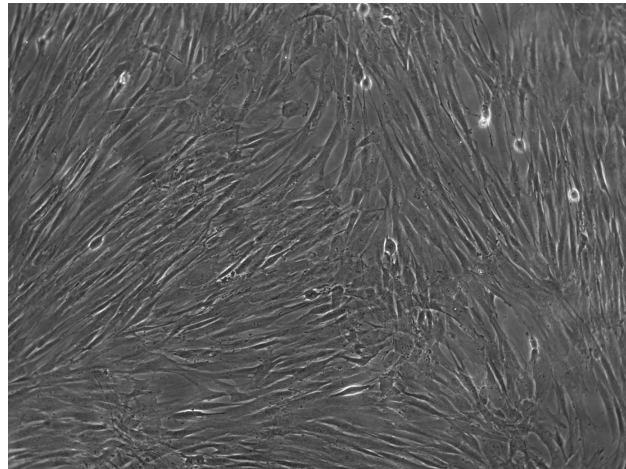
Difficulty seeding a consistent confluent monolayer

I seeded approximately 135,000 cells per well on a 6-well plate and let them grow for 24-48 hours before scratching the surface.

No peptide added to this confluency image taken after approximately 24 hours after plating.



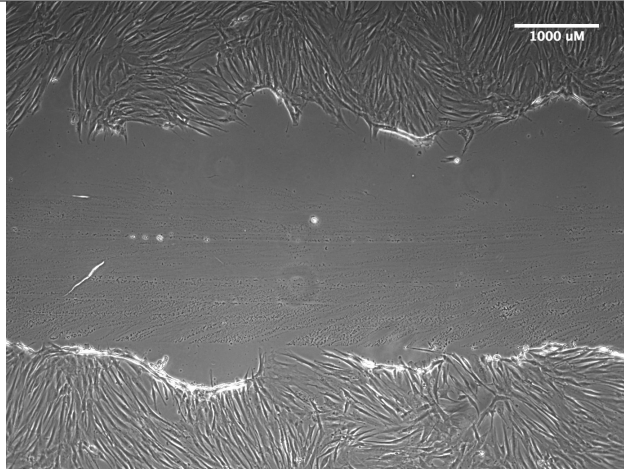
No peptide added to this confluency image after 48 hours from plating and before scratching.



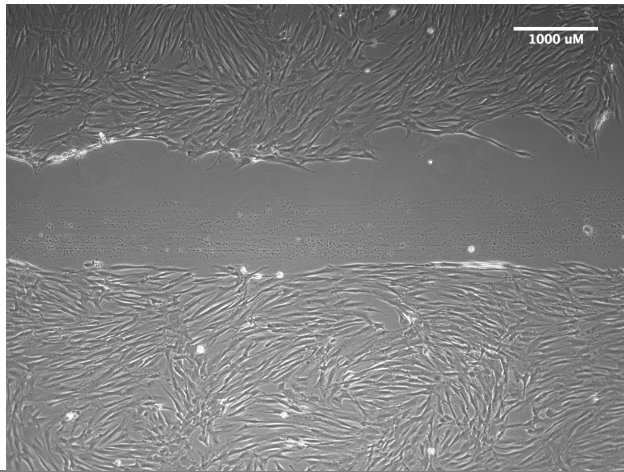
“Bad Scratches” made

A good scratch generally fits into the field of view for a 10x objective lens on the microscope you are using. The scratch has a consistent width throughout and is pretty straight across the well. A bad scratch would be either too big or very small. Also, a bad scratch would be wavy making it difficult to determine where the edge of the scratch is located.

Concentration of 12- μ M LL37 image of a “good” scratch taken at 0 hours



Concentration of 12- μ M LL37 image of a “bad” scratch taken at 0 hours



Time interval for collecting images

The scratches take around 24 hours to close so I took 5 different time points. Ideally more time points should be taken to see the scratch closing over time.

Location along scratch to take image

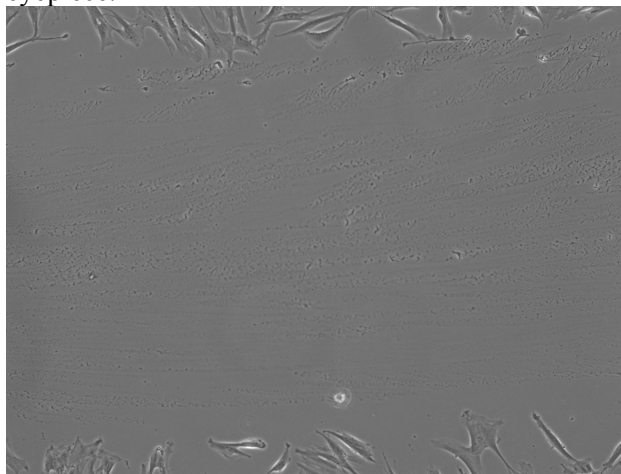
The entire length of the scratch does not fit onto the field of vision. When you are still trying to get consistent scratches I would take multiple pictures of each scratch and take one measurement per picture using ImageJ. When these measurements are similar it means your scratch is consistent and

I would then take three pictures per scratch and measure the scratch width in multiple locations (10) on each image using ImageJ. Note that it is important to never use an image near the edge of the scratch because the edge will always heal faster than the middle and could affect your scratch width over time.

Time period for a scratch to close completely

I found that a scratch with no AMP takes approximately 24 to 30 hours to close completely depending on the width of the scratch at the start. If the scratch is taking a much longer time to close then you scratched the surface of the tissue treated plate. This occurs when you press too harshly on the cells in order to scratch them. Scratching the tissue treated wells affects cell migration rates which is why it takes so long to heal the scratch. Usually you can see when you have pressed too hard on the surface because streaks and lines appear in the scratched area. Sometimes these streaks appear when the tissue treated surface has not been scratched but it is important to minimize the streaks.

Example of a scratched tissue treated well with no added peptide using a 5x objective lens and 10x eyepiece.



Cells are clumping on one area of the plate

This usually happens when you swirl the plate in a circular motion. Cells act like sand and will congregate because of this. Try instead shaking the plate back

and forth and side to side in order to evenly disperse the cells prior to incubating.

Adding peptide

With my experiments I added the peptide after scratching, rinsing, and adding media. This allows you to keep the peptide on the plate and not disturb the cells as much. Adding the peptide after also allows you to have to use less because you won't need to add more when you rinse the cells. A picture should be taken for time point zero immediately after peptide is added.

Out-of-focus cells in my microscope images

Rinse the cells once and then add media after scratching and before imaging. This will get rid of any cells that are floating in the scratch to make a better image.

Image of a scratch with no peptide added that was not thoroughly rinsed.

